AD-A098 044 NAVAL POSTGRADUATE SCHOOL MONTEREY CA F/G 8/14
CHARACTERISTICS OF GEOMAGNETIC POWER SPECTRA ON LAND AND SEA IN--ETC(U)
DEC 80 G M MCKINLEY, R M SANTOS

UNCLASSIFIED NL

END
DATE FILMED
5-81
DTIC

NAVAL POSTGRADUATE SCHOOL
Monterey, California

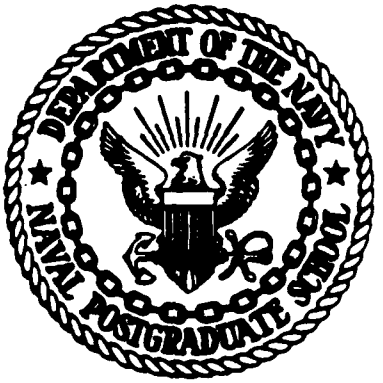

THESIS

CHARACTERISTICS OF GEOMAGNETIC
POWER SPECTRA ON LAND AND SEA
IN THE PERIOD RANGE
0.2 TO 400 SECONDS

by

Gary M. McKinley
and
Robert M. Santos

December, 1980

Thesis Advisor: P. Moose

Approved for public release, distribution unlimited

SECURITY CLASSIFICATION OF THIS PAGE (When Data Entered)

REPORT DOCUMENTATION PAGE	READ INSTRUCTIONS BEFORE COMPLETING FORM
1. REPORT NUMBER	2. GOVT ACCESSION NO. AD-A098 044	3. RECIPIENT'S CATALOG NUMBER
4. TITLE (and Subtitle) Characteristics of Geomagnetic Power Spectra on Land and Sea in the Period Range 0.2 to 400 seconds	5. TYPE OF REPORT & PERIOD COVERED (9) Masters Thesis; December, 1980
	6. PERFORMING ORG. REPORT NUMBER
7. AUTHOR(s) (10) Gary M. McKinley, Robert M. Santos	8. CONTRACT OR GRANT NUMBER(s)
9. PERFORMING ORGANIZATION NAME AND ADDRESS Naval Postgraduate School Monterey, California 93940	10. PROGRAM ELEMENT, PROJECT, TASK AREA & WORK UNIT NUMBERS (12) 131
11. CONTROLLING OFFICE NAME AND ADDRESS (11) Naval Postgraduate School Monterey, California 93940	12. REPORT DATE Dec [redacted]80
	13. NUMBER OF PAGES 92
14. MONITORING AGENCY NAME & ADDRESS(if different from Controlling Office)	15. SECURITY CLASS. (of this report) Unclassified
	15a. DECLASSIFICATION/DOWNGRADING SCHEDULE

16. DISTRIBUTION STATEMENT (of this Report)

Approved for public release; distribution unlimited

17. DISTRIBUTION STATEMENT (of the abstract entered in Block 20, if different from Report)

18. SUPPLEMENTARY NOTES

19. KEY WORDS (Continue on reverse side if necessary and identify by block number)

Low frequency geomagnetic measurements
Geomagnetic fluctuations, land and sea

20. ABSTRACT (Continue on reverse side if necessary and identify by block number)

Geomagnetic field fluctuations in the 0.025-5Hz range were measured with a Cesium vapor magnetometer on the sea floor in Monterey Bay, and at a remote land site. Correlation was found between the geomagnetic activity A-index and both the slope and relative magnitude of the power spectra. More active days showed a greater fall-off as frequency increased, and a higher level of the observed power spectra.

DD FORM 1 JAN 73 1473 (Page 1) EDITION OF 1 NOV 65 IS OBSOLETE S/N 0102-014-6601

SECURITY CLASSIFICATION OF THIS PAGE (When Data Entered)

Fluctuations averaging $0.1 nT^2/Hz$ were noted at the low frequencies, dropping to $10^{-5} nT^2/Hz$ at 1 Hz. Comparisons were made between the land/sea and day/night data to determine the sea and diurnal effects. In addition to swell induced fluctuations, the overall power spectra for sea data is 10-15 dB higher than land data. Diurnal shifts indicate a 20 second period increase in the nighttime Pc 3 fluctuations. Daytime intensity is generally 5 dB above the nighttime data, but with a crossover at 0.05Hz, the nighttime data then running 3 to 5 dB above the day. Further observations were made to determine the applicability of the magnetometer for non-seismic detection of nuclear blast.

Approved for public release; distribution unlimited

Characteristics of Geomagnetic Power Spectra on Land and Sea

in the Period Range 0.2 to 400 seconds

by

Gary M. McKinley
Lieutenant, United States Navy
B.S. in Geology, Tulane University, 1974

and

Robert M. Santos
Lieutenant, United States Navy
B.S., United States Naval Academy, 1974

Submitted in partial fulfillment of the

requirements for the degree of

MASTER OF SCIENCE IN PHYSICS

from the

NAVAL POSTGRADUATE SCHOOL
December, 1980

Authors: _____

_____

Approved by: _____
THESIS ADVISOR

_____
SECOND READER

_____
CHAIRMAN, DEPARTMENT OF PHYSICS AND CHEMISTRY

_____
DEAN OF SCIENCE AND ENGINEERING

ABSTRACT

Geomagnetic field fluctuations in the 0.025-5Hz range were measured with a Cesium vapor magnetometer on the sea floor in Monterey Bay, and at a remote land site. Correlation was found between the geomagnetic activity A-index and both the slope and relative magnitude of the power spectra. More active days showed a greater fall-off as frequency increased, and a higher level of the observed power spectra. Fluctuations averaging $0.1nT^2/Hz$ were noted at the low frequencies, dropping to $10^{-5}nT^2/Hz$ at 1 Hz. Comparisons were made between the land/sea and day/night data to determine the sea and diurnal effects. In addition to swell induced fluctuations, the overall power spectra for sea data is 10-15 dB higher than land data. Diurnal shifts indicate a 20 second period increase in the nighttime Pc 3 fluctuations. Daytime intensity is generally 5 dB above the nighttime data, but with a crossover at 0.05Hz, the nighttime data then running 3 to 5 dB above the day. Further observations were made to determine the applicability of the magnetometer for non-seismic detection of nuclear blast.

TABLE OF CONTENTS

LIST OF ILLUSTRATIONS

ACKNOWLEDGEMENT

As in any research effort, many people have contributed to this thesis. We would first like to thank our advisors, Professor Paul Moose and Professor Otto Heinz for their enthusiastic support and guidance. Also the Earth Physics Department of ONR for their partial support.

Our equipment was kept in operation thanks to the efforts of Mr. Robert Smith and Mr. William Smith of the Electrical Engineering Department. We would further like to thank Mr. Tom Maris and Mr. Ken Smith of the Physics and Chemistry Department for their help in keeping the system operating.

Finally, we would like to acknowledge the patience and support to our wives, who helped keep our spirits up when the workload got us down. Special thanks to Barbara Santos, typist extraordinaire.

I. INTRODUCTION

Studies of fluctuations of the earth's magnetic field ordinarily categorize these phenomena as either short or long period in nature. The long period fluctuations (on the order of years or more) are considered to be a part of the "main" magnetic field, an approximate dipole arrangement generated deep within the earth itself.

Short period fluctuations of about 1 part in 10^4 of the main field in magnitude are caused by wave-particle interactions in the magnetosphere and ionosphere. Other fluctuations are generated within the earth-ionosphere cavity. Sources which can be identified as due to lightning activity and high altitude nuclear blast have also been observed.

Sea based observations of both the main field and fluctuating field are complicated by two major factors. First, sea water is a good conductor when compared to the earth's crust. Secondly, there are anomalies associated with geological features of the sea floor.

The centuries old study of magnetic phenomena has been of historic interest to the Navy for several reasons. Perhaps the obvious is the use of the nearly constant main field for navigation. Furthermore, modern naval vessels have large magnetic signatures, which cause local fluctuations in the geomagnetic field. Magnetic sensors which detect these fluctuations

are used in triggering mechanisms of mines and torpedoes. Submarines also create an "anomaly" in the geomagnetic field, which can be detected with sufficiently sensitive equipment. Submarine communications at depth are possible at ELF frequencies using magnetic detectors.

All these applications require knowledge of the nature of the naturally occuring fluctuations in the local magnetic field. The primary thrust of this investigation has been to examine very low frequency fluctuations of the earth's magnetic field (.0025 to 5Hz) both at a remote land site (relatively free from commercial power transmission lines and other electromagnetic interference) and on the floor of Monterey Bay. In addition to increased understanding of the variety of magnetic fluctuations, it is postulated that there exists some correlation of land and sea data. If true, it will facilitate investigation of the possibility of the propagation of EM waves through the earth's crust and aid in the estimation of both sea floor and earth's crust conductivity.

The data collection system for this investigation was designed and tested by John Chaffee [1979]. It utilizes an optically pumped Cesium vapor magnetometer and small analog tape recorder. Some equipment difficulties were encountered which limited the amount of sea data recorded. The equipment was used to obtain a land data base suitable for future study.

II. BACKGROUND

A. GEOMAGNETIC FLUCTUATIONS

The geomagnetic field, as observed by the Cesium vapor magnetometer is composed of a nearly constant main field (Figure 1) upon which are superimposed a spectrum of geomagnetic fluctuations. The main field is approximately 50,000 nT in magnitude with the smaller field fluctuations on the order of 10 nT or less. Figure 2 illustrates, schematically, the main field and its fluctuating components as measured by the Cesium vapor magnetometer.

There are various types and durations of the earth's magnetic field fluctuations. Daily variations, also called diurnal, manifest themselves in variations of declination of a few minutes of arc and variations of intensity of between 20 and 50 nT. Larger variations, similar in period to the daily ones, are due to magnetic storms which cause shifts in declination of several degrees and very large intensity fluctuations. Impending storms can be distinguished by differing phases, the main phase characterized by a general reduction in intensity of as much as 100 nT below the undisturbed magnitude of the geomagnetic field.

Overall, the daily variations of magnetic field fluctuations are rapid transient changes due to electric current in the upper

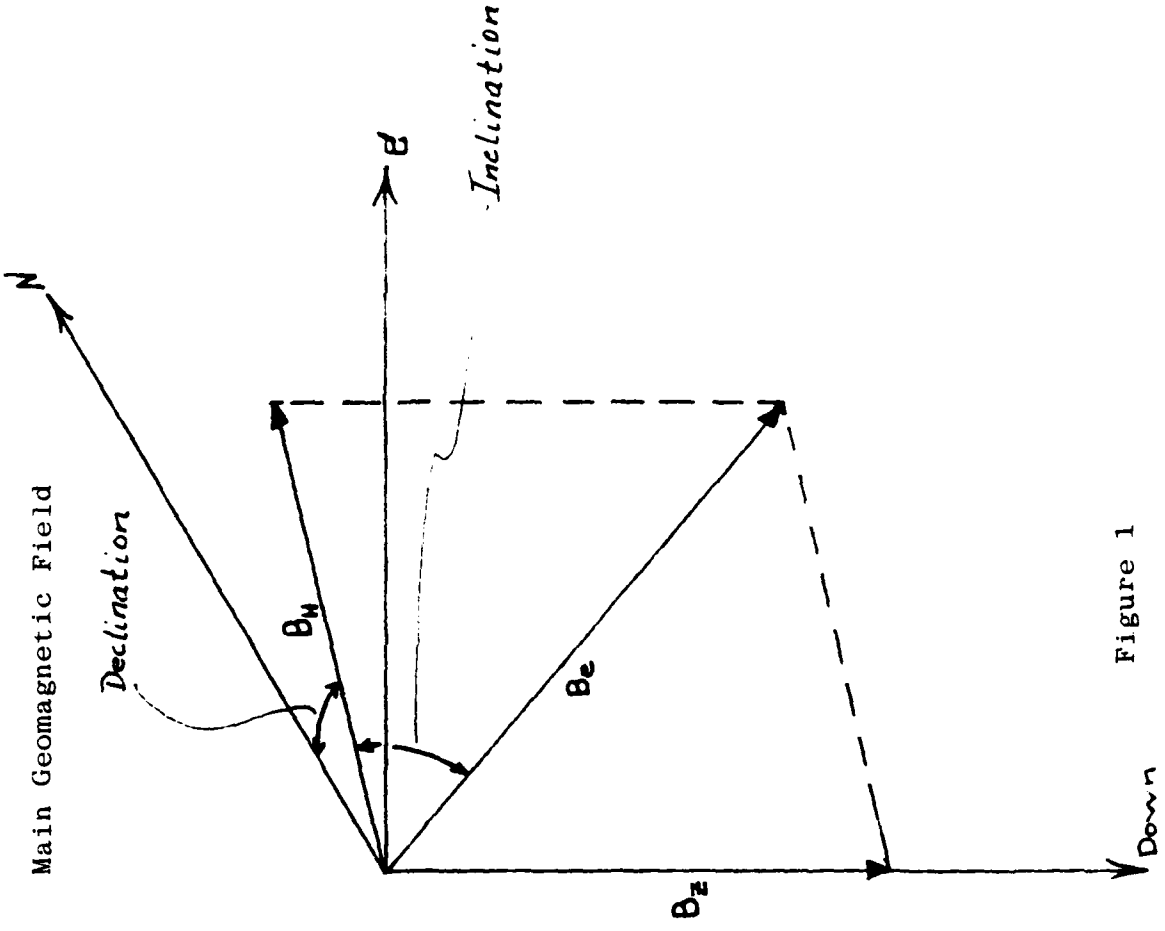
Main Geomagnetic Field
N
Declination
Inclination
D
B_H
B_e
B_z
Down

Figure 1

atmosphere. This is largely due to electrons in the ionosphere being stripped from oxygen and nitrogen by solar UV radiation. This makes the ionosphere an electrical conductor and subsequent electrical currents in the ionosphere cause the transient variations in the magnetic field [Takeuchi, Uyeda, Kanamori, 1970].

Geomagnetic fluctuations may be induced by other mechanisms such as resonant effects of lightning bursts in the ionospheric cavity of the earth [Schumann 1952], as well as effects due to atomspheric detonation of nuclear devices [Balser and Wagner 1963]. In the latter instance, the observed fluctuations are not associated exclusively with ionospheric cavity excitations. Another possibility, in this case, would be the ionization of the lower region of the ionosphere, which would appear as a fluctuation in the magnetic field similar to those observed as daily variations. Such a disturbance as this would have a longer observable effect than those of the more rapid transient cavity disturbances. The effects of the nuclear detonation might be difficult to distinguish from those of a diurnal nature, since the observable shift on peak power frequency due to asymmetry in the earth's ionspheric cavity are about the same for both daily variations and nuclear detonations.

Of particular interest is the class of geomagnetic fluctuations known as micropulsations. The International Association of Geomagnetism and Aeronomy define micropulsations as

fluctuations with periods in the .1 second to 600 second range. These micropulsations are categorized as either continuous or irregular (Figure 3). Irregular micropulsations are associated with polar magnetic disturbances and are observed as nighttime phenomena. These irregular micropulsations are broken down into Pi 1 (1-40 second period) and Pi 2 (40-150 second period). It is suspected that these arise from conductivity disturbances of the ionosphere, in turn due to particle bombardment from the magnetosphere as well as increased solar radiation levels. They are often correlated with polar aurora and cosmic radio noise absorption.

Smoothly varying pulsations with oscillatory periods are classified as "continuous" or Pc micropulsations. These pulsations are divided into five categories Pc 1 to Pc 5:

a) Pc 1: [.15-5 second period] These are associated with solar disturbances and have been studied as a means for possible prediction of impending magnetic storm activity [Frasier-Smith 1979].

b) Pc 2 and Pc 3: [5-10 seconds and 10-45 seconds respectively] The amplitude is usually less than .5 nT for Pc 2 and Pc 3. These are diurnal phenomena showing some correlation with solar activity and seasonal effects. They may fall in period from 20 seconds to 10 seconds with the day to night transition.

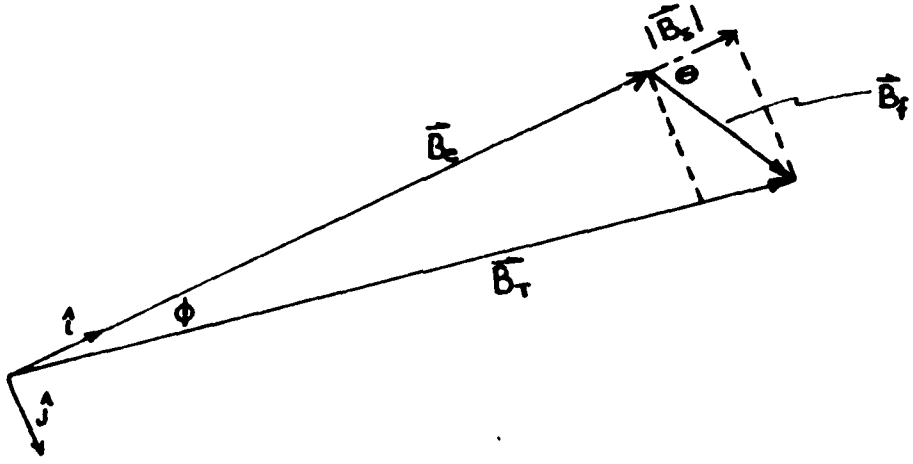

$\vec{B}_e$ - Earth's magnetic field vector
$\vec{B}_T$ - Total magnetic field vector
$\vec{B}_f$ - magnetic fluctuation vector

$|\vec{B}_s|$ - magnitude of signal vector measured by the magnetometer
ϕ - deviation of $\vec{B}_T$ from $\vec{B}_e$
θ - deviation of $\vec{B}_f$ from $\vec{B}_e$

Fluctuations Imposed on the Main Geomagnetic Field

Figure 2

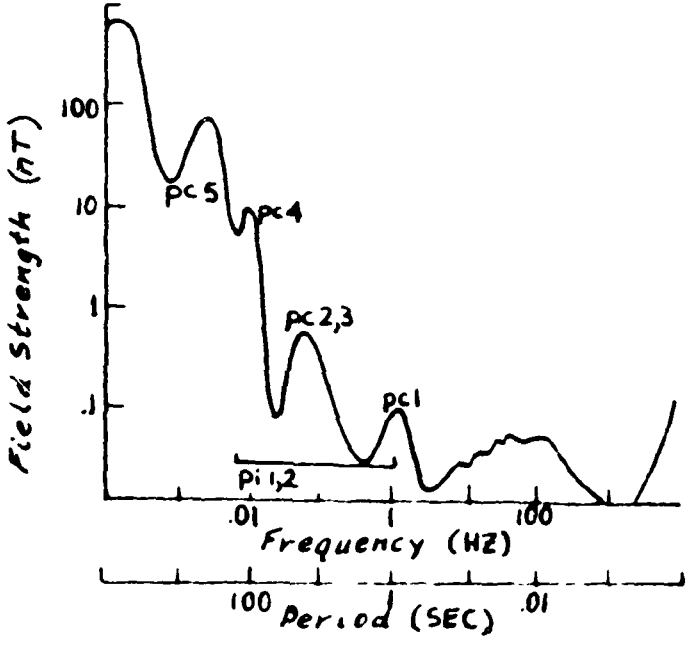

Field Strength of Micropulsations

Figure 3

c) Pc 4: [45-150 second period] Pc 4 is associated with sunspot activity and has been observed to change in period with seasons (possibly due to atmospheric density variations).

d) Pc 5: [150-600 second period] These are large amplitude variations of, at times, several hundred nanoteslas, and are somewhat larger as morning events. They are most evident in between magnetically active periods.

The fluctuations measured by the Cesium vapor magnetometer represent the magnitude of the signal vector, B_S, shown in Figure 2. This magnitude is the projection of the field fluctuation vector, B_f, onto the earth's magnetic field. This can be shown as follows:

From Figure 2,

$$\vec{B}_e = B_e\hat{\imath}$$

$$\vec{B}_f = B_f\cos\theta\hat{\imath} + B_f\sin\theta\hat{\jmath}$$

therefore,

$$\vec{B}_T = \vec{B}_e + \vec{B}_f = (B_e + B_f\cos\theta)\hat{\imath} + B_f\sin\theta\hat{\jmath}$$

and,

$$B_T^2 = B_e^2 + 2B_eB_f\cos\theta + B_f^2\cos^2\theta + B_f^2\sin^2\theta$$

Because the field fluctuation is on the order of 10^{-4} that of the earth's field, i.e., $\vec{B}_e >> \vec{B}_f$ the last two terms can be neglected;

$$B_T^2 - B_e^2 = 2B_eB_f\cos\theta$$

$$(B_T + B_e)\ (B_T - B_e) = 2B_eB_f\cos\theta$$

Then $B_T - B_e = B_s$ and $B_T + B_e \simeq 2B_e$

therefore,

$$2B_eB_s = 2B_eB_f\cos\theta$$

and,

$$B_s = B_f\cos\theta$$

or written in vector form;

$$|\vec{B}_s| = \frac{\vec{B}_e \cdot \vec{B}_f}{|\vec{B}_e|} = \hat{1} \cdot \vec{B}_f$$

Notice that the measurement of $|\vec{B}_s|$ as the magnitude of the geomagnetic field fluctuation is valid with the understanding that the value of ϕ (see Figure 2) is very small, and the magnitude of the earth's field with respect to the magnitude of the fluctuation is very large.

B. ACTIVITY INDICES

The geomagnetic activity is continuously monitored by solar and magnetic observatories and the degree of activity is represented by the K-index for a three hour time interval based on a scale of 0 (least active) to 9 (most active). Since

the K-index is not linear, the A-index is a more useful representation of the daily activity and is derived from the K-index by using conversion tables. The A-index is listed along with the K-index for individual days, in weekly reports available from the Space Environment Services Center in Boulder, Colorado. A detailed description of these indices is discussed by Lincoln in Physics of Geomagnetic Phenomena Vol. I.

Very often, it is of more use to consider the daily activity with respect to an average value of the A-indices over the period of interest [Frasier-Smith, 1979]. In this way a quick comparison of the relative field intensity can be obtained for any observation taken during that time.

C. CRUSTAL CONDUCTIVITY

The measure of the crust's ability to transfer a charge in response to a given impressed electromagentic force is its conductivity. A detailed discussion of the processes and theory involved in the determination of the conductivity of the upper layers of earth crust, in several modeled formats, is contained in early work by Sunde (1949). Initial studies observed the magnetic field generated by direct current in wires between point electrodes. Periodic reversals of current and resultant variations of the magnetic field give rise to inductive effects. This early work produced some broad

observations of conductivity of the earth crust for different constituent crusts and geologic periods.

The conductivity of the earth's crust is easier to determine by direct measurement, thus making sea sediment measurements most cumbersome to obtain [Ewing, Press, 1955]. Duffus, Shand and Wright (1961) note the effect of sea/land conductivity discontinuities on their measurements of geomagnetic component fluctuations in the .001 to 1Hz frequency range. By measuring the magnetic field intensity simultaneously on land and at sea, it should be possible to identify the portion of the power density spectrum measured at sea which does not appear on land. From this knowledge it may be possible to determine the amount of the magnetic field which is transmitted up through the sea floor crust and subsequently make estimates concerning the crustal conductivity of the sea floor.

D. THE OCEAN ENVIRONMENT

Other factors contribute to the power density spectrum observed in measurements of the geomagnetic fluctuations in the sea environment. Propogation of electromagnetic radiation in the conducting medium of sea water and sea bottom effects, must be anticipated to accurately predict the geomagnetic field variations that occur in this region. Making the assumptions that the model of a three layer medium applies, which is composed of air, sea, and sea bottom, all non-magnetic,

and with the sea and sea bottom acting as good conductors, it can be shown that attenuation in the ocean of frequencies above 100Hz render these signals undetectable to the Cesium magnetometer [Chaffee, 1979]. Additionally, at very low frequencies and shallow depths, the amplitude of the field fluctuations are actually greater than those incident upon the air/sea interface.

Further consideration must also be given to those fluctuations of the magnetic field generated by the sea wave activity of the ocean. Wave noise has an appreciable influence on measurements in the sea, provided the appropriate sea conditions for swell and wave height exist. It has been shown theoretically and from empirical observation that long period swell can have a significant influence on the magnetic intensity [Weaver, 1965].

E. PREVIOUS WORK

High sensitivity measurements of field fluctuations, on land in the .1 to 14Hz range using a super-conducting magnetometer, were made by Frasier-Smith and Buxton in 1975. This work focused, primarily, on the Pc 1 micropulsations and provides an excellent reference for the slope of the power density spectrum of total geomagnetic field fluctuations. In particular, the studies showed an overall decline in the amp-

litude of nighttime events relative to daytime and that the increase or decline of the power spectrum, respectively, lags local sunset or sunrise by approximately three hours.

Baseline land data was produced locally by Barry (1978) using a Cesium vapor magnetometer for subsequent use of that system in an underwater configuration in Monterey Bay, California. These observations were in general agreement with the earlier studies of Frasier-Smith and Buxton for the same frequency ranges. In addition, relationships between night and day activity and excited and unexcited geomagnetic periods were examined.

The initial local underwater experiments were performed by Chaffee (1979), in Monterey Bay, California, establishing the functional configuration of the sea floor sensing system currently in use and exploring the potential use of the system in a deep water environment. Observations were made of the influence of sea wave and swell on the geomagnetic power density spectrum.

Wave induced phenomena were highlighted in the .05 to 1Hz frequency range and events of 67 seconds in period were examined for possible correlation with Pc 4 events or long ocean wave induced effects.

McDevitt and Homan (1980), using a coil sensor, made land and sea measurements of the horizontal component of the

magnetic field fluctuations and also attempted to measure the vertical component. It was discovered that the magnitude of the vertical component was below the sensitivity of the coil system; however, it was possible to place an upper limit on the vertical component of 10^{-3} nT^2/Hz at 1Hz and 10^{-6} nT^2/Hz at 10Hz. It was found that determining the actual orientation of the coil on the sea floor is extremely difficult in both the vertical and horizontal planes. Any deviation of the axis of the coil from vertical while set in the horizontal plane is particularly critical.

III. EQUIPMENT DESCRIPTION

A. DATA COLLECTION SYSTEM

1. Basic Component Description

The major components of the data collection system (see Figures 4 and 5) are listed below:

a) Cesium vapor magnetometer (Varian Associates Model 4938)

b) Sensor Coupler (Varian Model 4938)

c) 2 KHz reference oscillator

d) 2 Channel Analog Cassette Recorder (Marantz Model CD330)

e) Frequency to Voltage Discriminator (Anadex Model P-375)

f) Voltage Controlled Oscillator

g) Batteries (Gould Gelyte Cells)

The Magnetometer generates a signal whose frequency varies proportionally with the intensity of the local magnetic field. In the Monterey area, the main field frequency (called the Larmour frequency) is on the order of 176.5 KHz. The Larmour frequency output of the sensor is transmitted through a coaxial cable to the sensor coupler. It is there mixed with a crystal oscillator to generate a difference frequency between 0 to 2000Hz. This difference frequency is fed into the frequency to voltage discriminator which provides a voltage out proportional to the frequency of the input. The voltage output of the discriminator is fed to the voltage

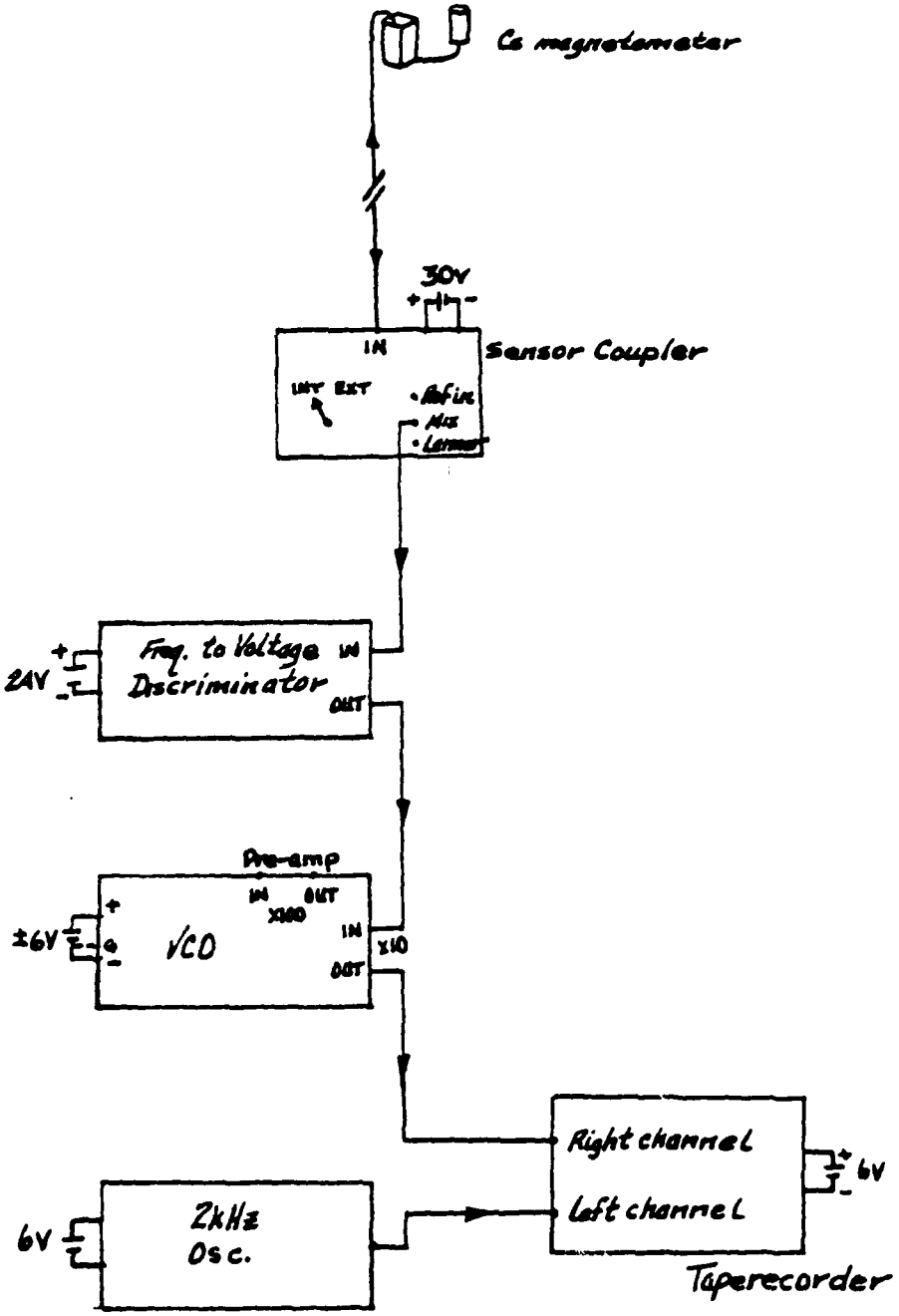

Data Collection Equipment

Figure 4

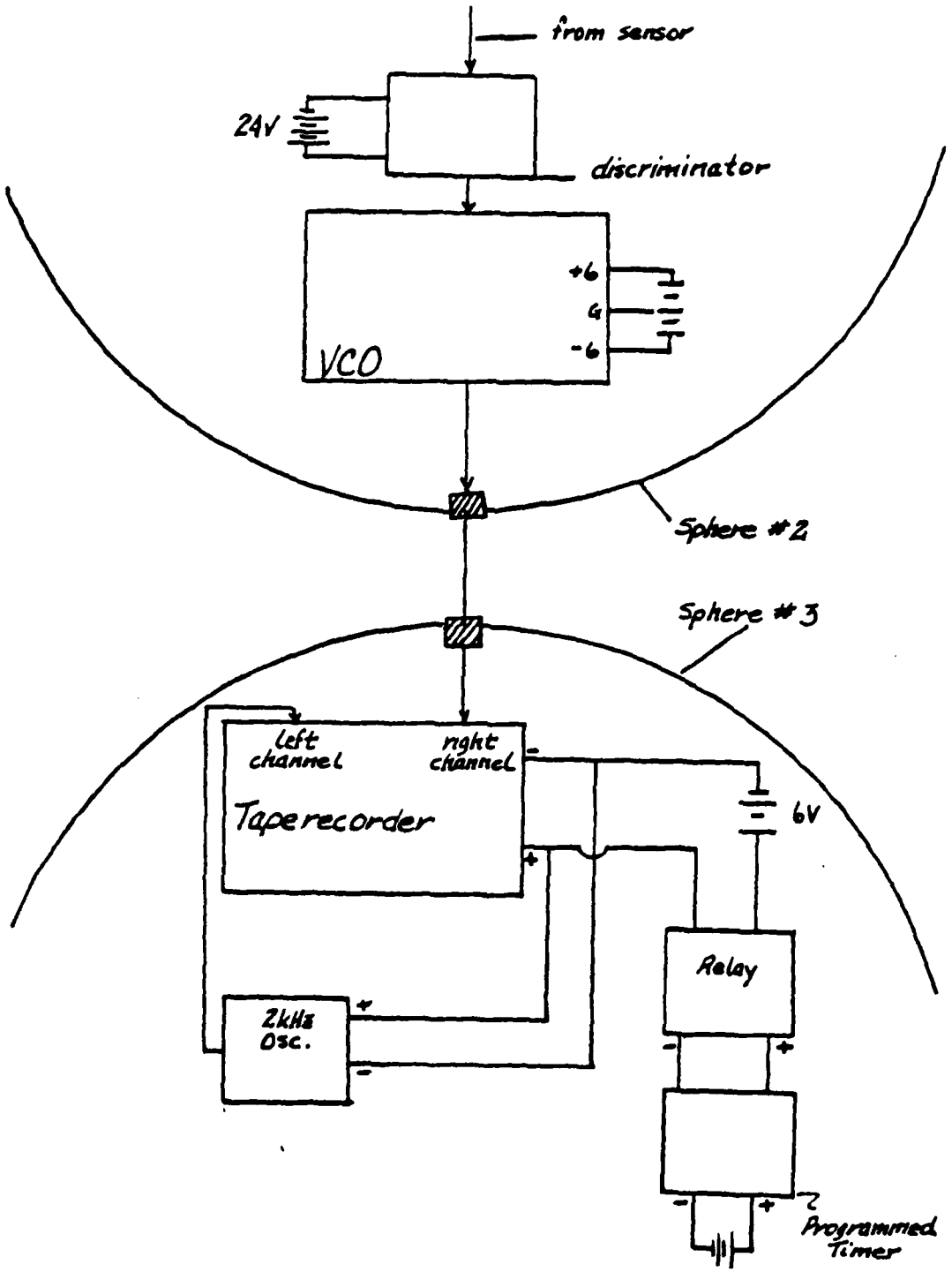

Data Collection Equipment

Figure 5

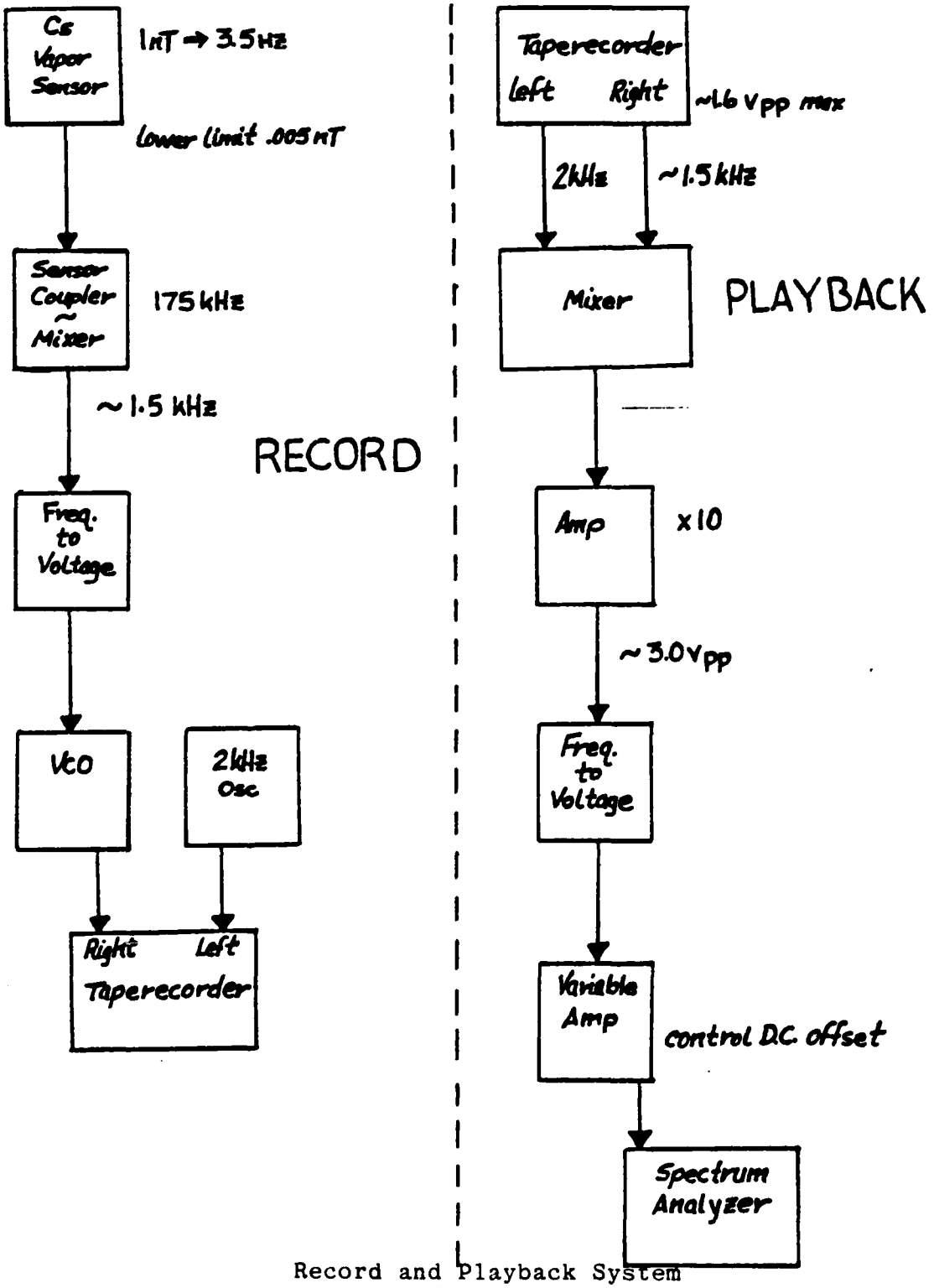

Record and Playback System
Figure 6

controlled oscillator (after AC coupling). The voltage controlled oscillator generates a sinusoidal waveform varying about 1.5 KHz. The frequency variation of the VCO output is therefore analogous to the fluctuations of the sensor output frequency and thus represents the magnetic field fluctuation. This VCO output is fed into one channel of an analog cassette recorder.

This system arrangement relates a 122Hz frequency shift to a 1 nanotesla (1nT) field strength, as opposed to the 3.5Hz/nT sensitivity at the sensor coupler.

The second input to the tape recorder is a 2 KHz reference oscillator signal.

Power Supplies for all the equipment are Gould Gelyte batteries. They are constructed of non-magnetic materials and have sealed, non-spill electrolyte making them ideal for undersea applications.

B. DATA REDUCTION SYSTEM

1. The data reduction system components (see Figure 6) are listed below:

a) 2 channel analog cassette recorder (Marantz Model CD-330)

b) 2 KHz Reference Oscillator

c) Amplifier

d) Frequency to Voltage Discriminator (Anadex Model P-375)

e) Spectrum Analyzer (Nicolet Scientific Mini Ubiquitous Model 440-B)

f) Tektronix amplifier

The cassette tape containing the recorded data channels is played into the mixer. The mixing of the data channel with the 2 KHz reference oscillator channel serves to reduce the tape recorder noise (wow and flutter). The system as designed requires 10dB gain to drive the discriminator.

The amplitude of the data signal into the spectrum analyzer must be adjusted so as not to overload the input amplifiers. Such an overload adversely effects the averaging process of the analyzer.

C. SEA DATA COLLECTION SYSTEM

1. Description

The basic sea data collection system places the sensor in a sealed glass sphere which is then attached to a non-metallic anchoring device. This anchor/sensor combination weighs approximately 400 pounds. It is connected via nylon line and coaxial cable to the remaining electronics equipment and recovery buoys.

The electronics spheres are placed in an aluminium bracket, and connected as shown in Figures 7 and 8 for data collection. Three spheres are used, one for the sensor coupler and power supplies, another for the VCO and Discriminator, with their batteries, and a third for the recorder package. This setup requires that only the recorder sphere be opened between data runs.

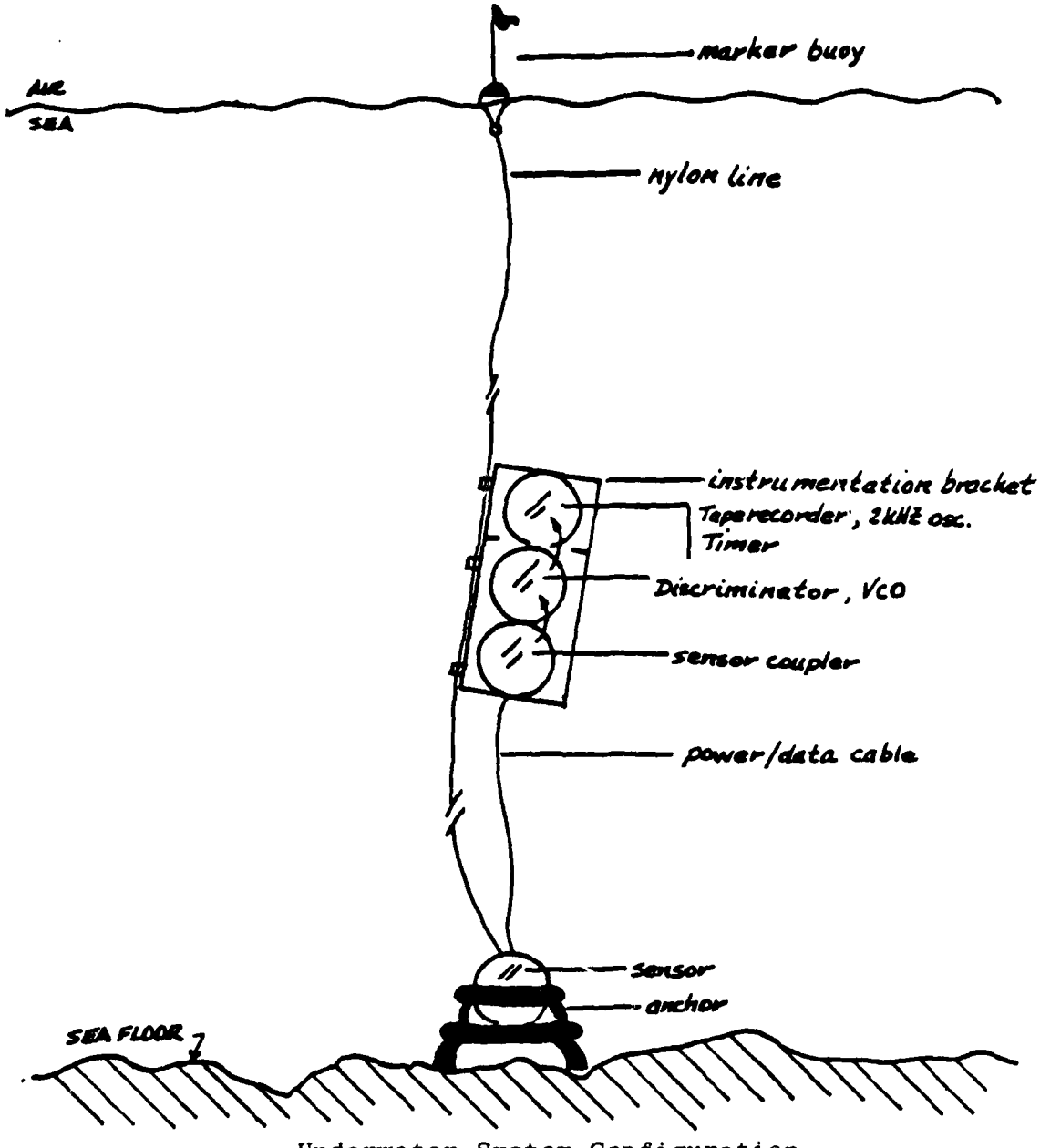

Underwater System Configuration
Figure 7

Launching of Instrumentation Package

Figure 8

These three spheres represent a significant improvement over a two sphere configuration. There is more room for battery power in each sphere, allowing use of larger (both amp-hour and size) batteries. Also, the decreased packaging density allows for more rugged packaging. Of course, any improvement involves trade-offs. The increased size and weight of the data collection system places it at the practical size limit for safe handling in significant sea states from the R/V Acania.

2. Packaging

The packaging of the equipment in the glass spheres is a very important aspect of the experimental work. Primary concerns in this area are equipment security and watertight integrity.

Two methods are used to keep equipment secure within a sphere, suction cups and styrofoam templates. Both methods prevent equipment motion during launch and recovery operations, as well as preventing any shifts due to wave action while the system is deployed. The suction cups are preferred for the lighter pieces; the pre-cut styrofoam templates are preferred for use with the heavier batteries.

Watertight integrity poses a need for greater care during any phase of handling the glass spheres. The ground glass edges are quite fragile, and the slightest chip render them useless for deep water experiments.

Prior to placing instruments in the spheres, all penetrators must be checked for tightness and electrical continuity. The top and bottom hemispheres must match serially.

After the equipment is properly secured within the sphere, the final step of sealing the sphere is accomplished (see Figure 9). The mating surfaces must be kept scrupulously clean and dry. Excess sealant compound and tape residue must be removed with Tolulene prior to application of new sealant and tape. Drying can be speeded with a high capacity heat gun (again, watch the glass edges). The mating arrows must be in line prior to resealing. Care must be taken to center the sealing compound strip along the "seam" of the sphere mating surfaces. Several turns of wide sealing tape finish the job.

3. Launch/Recovery

In general, the launch and recovery of the equipment is overseen by the crew of the R/V Acania. Once the coaxial cable is attached between the sensor coupler and sensor, all other connections can be made and excess cable secured to the equipment frame to prevent fouling. The securing of the coaxial cable to the nylon line must be done with the line under tension, as the elongation of the line under tension causes undue stress at the connectors (see Figure 10).

Packaging of Underwater Collector System

Figure 9

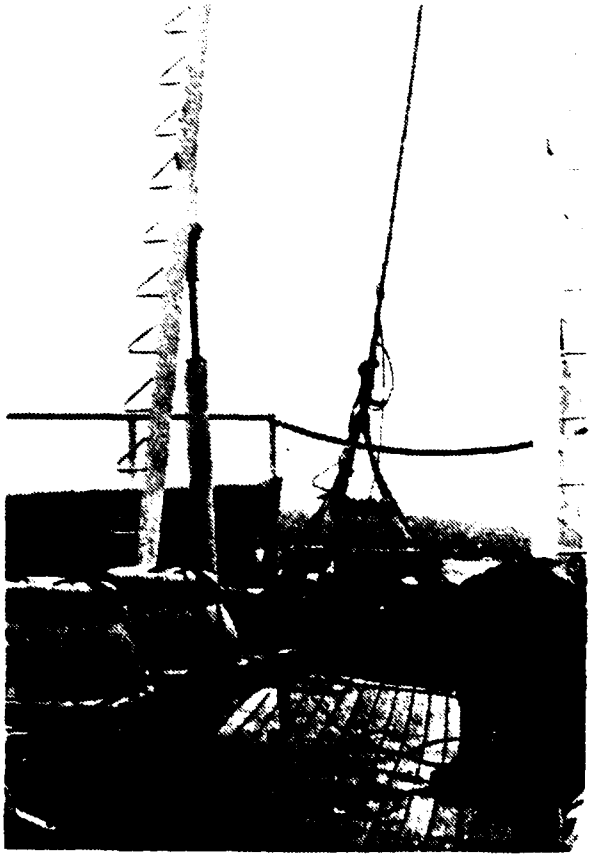

The use of a timing device allows the Acania to clear the area prior to equipment activation. Upon completion of the data collection run, the Acania proceeds to the sensor and commences the recovery operation.

When the equipment is retrieved, only the recorder package need be opened. Once the sphere is opened, the cassette is replaced and timer reset. The sphere must be dried internally to remove any condensation prior to further data collection runs. At this point, the sphere can be resealed and readied for another launch.

D. LAND DATA COLLECTION SYSTEM

The land data collection system is identical to that used for the sea data. However, there no longer is a requirement to enclose the equipment in glass spheres. This makes the equipment much more portable. Care must be taken to keep the equipment as free from dust and dirt as possible.

The sensor is sensitive to heat so care must be taken in choosing its location. Direct sunlight will cause overheating, so a well ventilated area is required. If a sun shield is rigged, a tent arrangement is desired to allow airflow around the sensor. Maximum operating temperature is approximately 50°C (122°F).

As stated in the battery description, the battery life decreases at low temperatures. It was found during night

operations near 35°F, battery life was half the normal encountered in daytime operations. Some thermal protection is therefore desireable for any long-term magnetic observatory using these power sources.

E. SYSTEM PERFORMANCE

1. System Transfer Function

Figure 11 represents the overall system transfer function. The method of obtaining this curve is detailed in Appendix A. The significance of this curve is apparent at the lower frequencies. The A-C coupling introduced in the VCO input stage to prevent overdriving the system also attenuates this low frequency data. The transfer function value is added to the data to account for the attenuation.

2. System Noise Curve

Figures 12 and 13 represent the noise generated by the system components. It is noted that the noise spikes beginning at approximately 3Hz are a dominating factor. They are attributed to noise generated by the tape recorder drive motors.

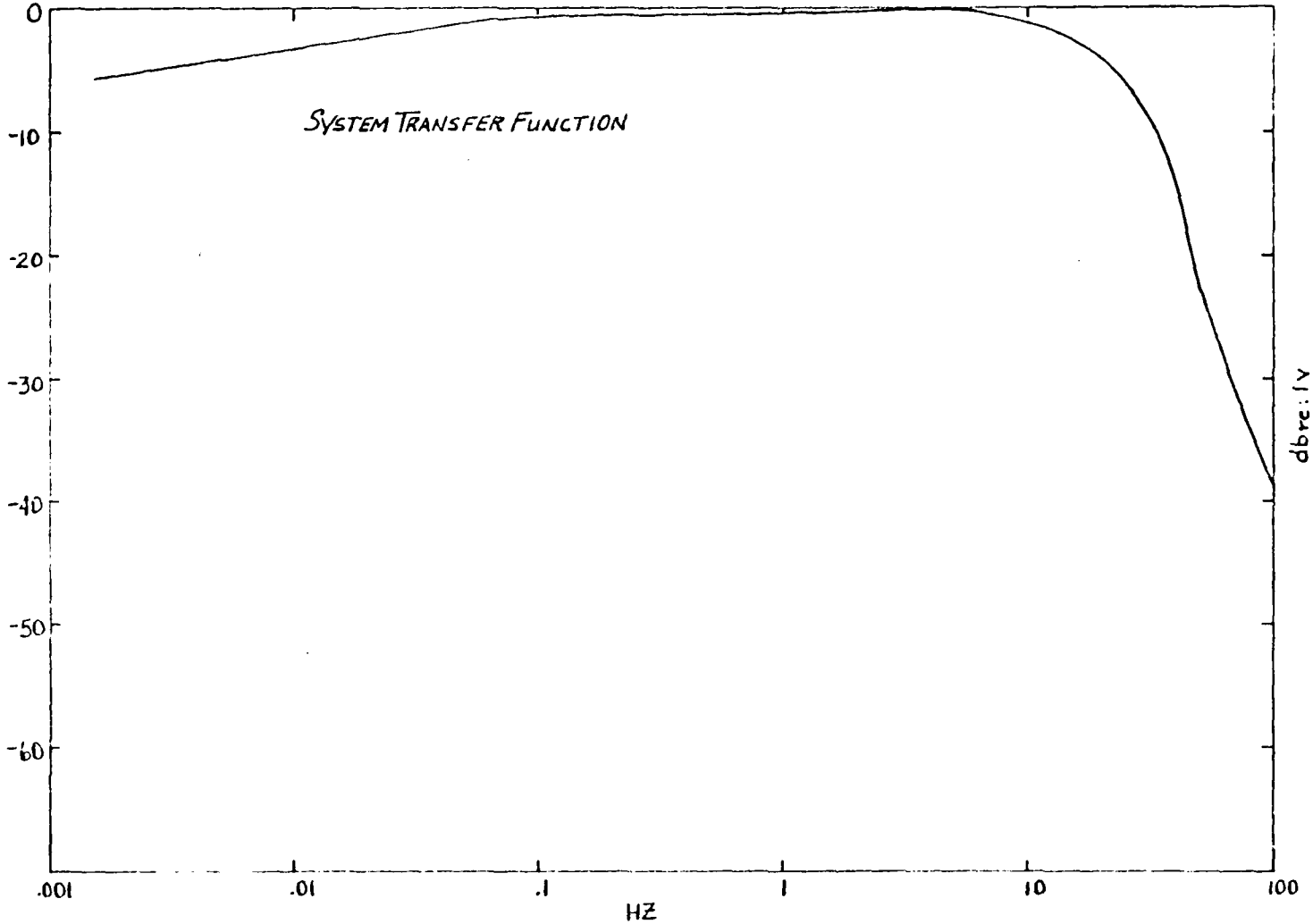
SYSTEM TRANSFER FUNCTION
0
-10
-20
-30
-40
-50
-60
.001
.01
.1
1
10
100
HZ
dbre: 1v

Figure 11

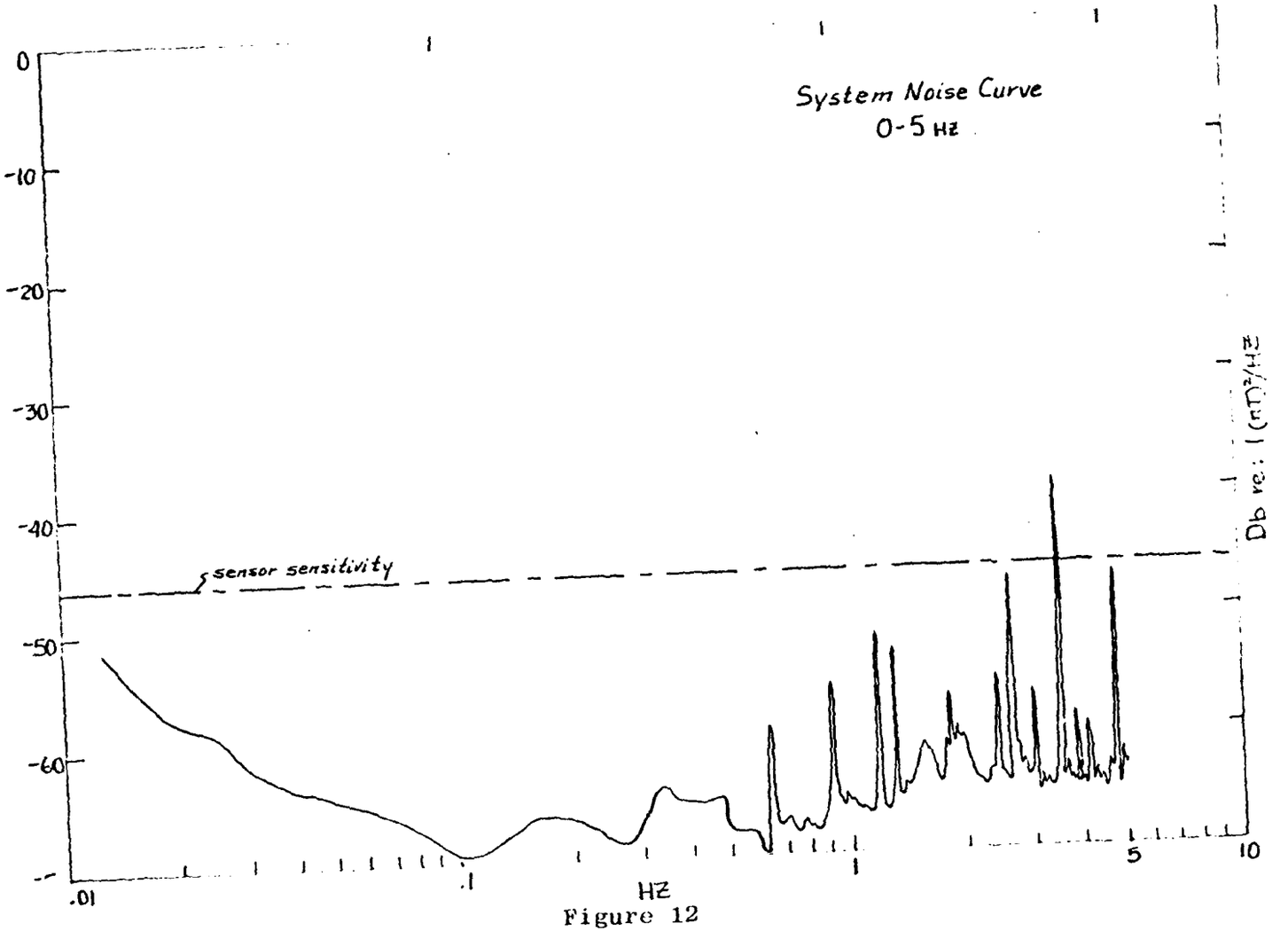
System Noise Curve
0-5 Hz
0
-10
-20
-30
-40
-50
-60
sensor sensitivity
.01
.1
1
5
10
HZ
db re: 1 (nT)²/HZ
Figure 12

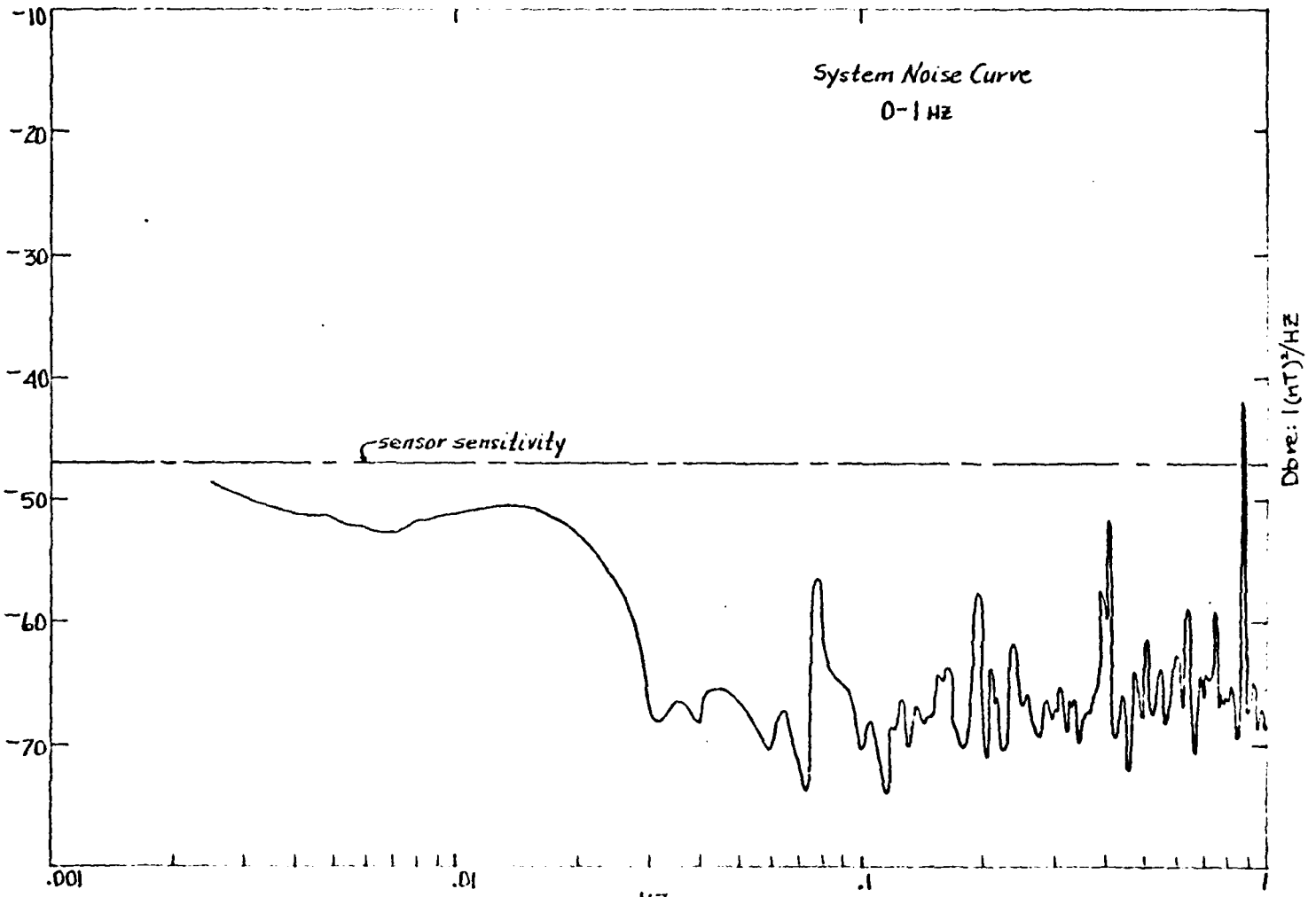
System Noise Curve
0-1 Hz
-10
-20
-30
-40
-50
-60
-70
sensor sensitivity
Dbre: 1(nT)²/Hz
.001
.01
.1
1
Hz
Figure 13

IV. EXPERIMENTAL RESULTS

The recorded data was frequency analyzed in order to examine the power spectrum of the magnetic field fluctuations. The power spectra were studied individually to find the trends of the curves. Additional comparisons of the data were facilitated by averaging the values of the power spectra for similar times and locations of data collection.

A. ANALYSIS OF INDIVIDUAL DATA RUNS

Spectra were obtained for the individual data tapes in two frequency bands, 0-1 and 0-5Hz. The 0-5Hz band (Figures 19-34) seems to be dominated by two limiting factors; first, the system noise above 1Hz and, second, the sensor sensitivity above 0.5Hz. The large noise spikes are thought to be generated by the tape recorder drive motor.

The 0-1Hz band (Figures 35-38) were analyzed to obtain greater resolution for the lower frequency portions of the power spectra. There are still noise spikes which dominate the 0.1 to 1 Hz portion of the spectrum, and a broadband noise pulse exists between .007 and .03Hz. These high noise regions can mask data. In general however, the curves remain well above the sensor sensitivity throughout this frequency band.

Figure 14 is a daily plot of the A index over the time frame of data collection. As expected, the relative amplitudes of the spectra seem to vary with the A index. The data taken on the 25th of July represents a period when the A index was over 30, the level considered to be a magnetic storm. The A index on the 17th of October was near the average value of the index over the entire data collection period. Figures 22 and 23 are referenced for direct comparison of average and active day spectra.

1. Discussion 0-5Hz

Previous investigators have noted a decrease in the power spectrum with increasing frequency (Figure 3) of approximately 30dB per decade. The data shows an average fall-off of approximately 29dB per decade. This fall-off appears to vary directly with the A index. That is to say, the greater the geomagnetic activity, the greater the fall-off of the power spectra. This observation conforms with the observations of Nishida (1978). More active days tend to manifest themselves by attenuating the higher frequency pulsations and enhancing the lower frequency pulsations (Pc 3, 4, and 5).

2. Discussion 0-1Hz

The 0-1Hz data curves (Figures 35-38) continue to show the expected fall-off in the power density with increasing frequency. The fall-off does appear to be slightly less than both the theoretical and the observed 0-5Hz fall-off. The

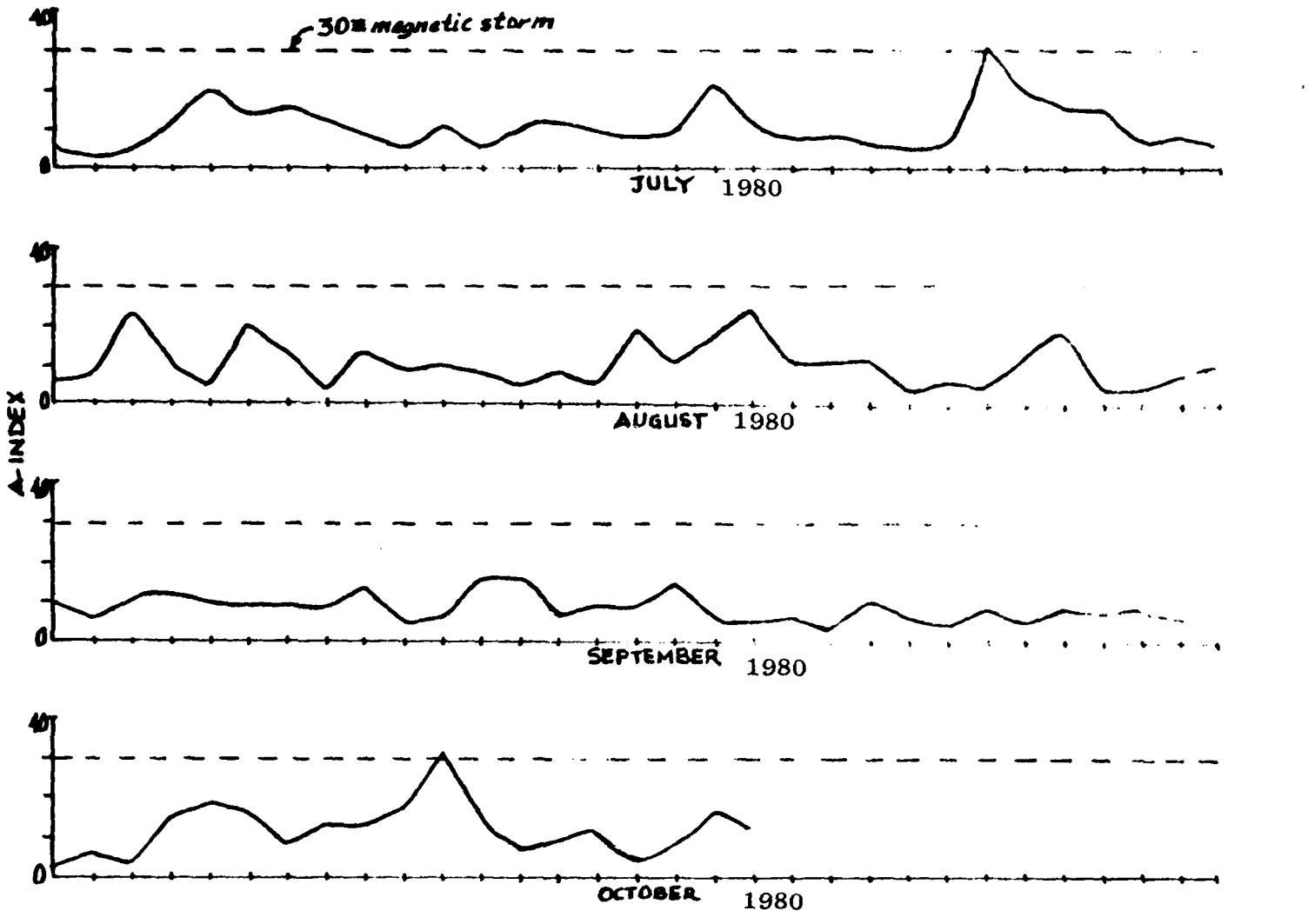
40
30≥ magnetic storm
0
JULY 1980
40
0
AUGUST 1980
A-INDEX
40
0
SEPTEMBER 1980
40
0
OCTOBER 1980
1 2 3 4 5 6 7 8 9 10 11 12 13 14 15 16 17 18 19 20 21 22 23 24 25 26 27 28 29 30 31 DAY

Figure 14

average A index (normalized to the average over the collection period) for these curves is 1.15. This is slightly less than the index over the period of the 0-5Hz data, so the decreased fall-off is thus expected.

Examination shows a prominent pulse at both the expected locations of the Pc 4 and the Pc 2, 3, micropulsations. As one would expect, the relative amplitudes of the pulsations vary with the A index. The more active days favor the lower frequency pulsations [Nishida, 1978].

The sea data curve (Figure 37) exhibits a unique high amplitude pulse near 0.08Hz. This related to the 10-14 second swell period noted on the day the data was collected.

B. COMPARISON OF LAND AND SEA DATA

In Figure 15, the average power densities for land and sea data are plotted. The curve for the sea data is based on 7 observations covering 3.5 hours, and the land data curve is based on 10 observations covering 5 hours of data collection. The sea data includes 2 hours of data collected on previous experiments using the same equipment [Chaffee, 1979] that was used for the collection of land and sea data over the period 21 July to 19 October, 1980.

A power density peak can be noticed in the sea data near 0.07Hz. This corresponds to a 14 second period for the pulsations noted. The two curves are roughly parallel with

the exception of the sea swell generated peak. It is interesting to note the sea data curves have a higher power density than the land data. This is believed to be caused by the large amount of background noise in the Monterey area.

In particular, note the increase in the field intensity (see Figure 15) in the 0.02 to 0.1 frequency range (Pc 3) for the sea data comparison to the land data. This suggests the influence of sea water as a conductor for these low frequencies and at the shallow depths of water in which the data was recorded (approximately 80 meters). Chaffee (1979) notes these effects and predicts the increase in the induced field at the sea floor with respect to the incident field for the frequency range and water depth of the average sea data shown in Figure 15.

It is impossible to specifically identify the contribution of each possible phenomenon that affects the resultant greater power density of the sea data since the observations on land and at sea were not taken simultaneously. It is possible to identify the contribution of sea swell affects on the average sea spectrum at approximately 0.07Hz. This appears as a sharp peak at this frequency in the sea data in contrast to the smoother average land data spectrum.

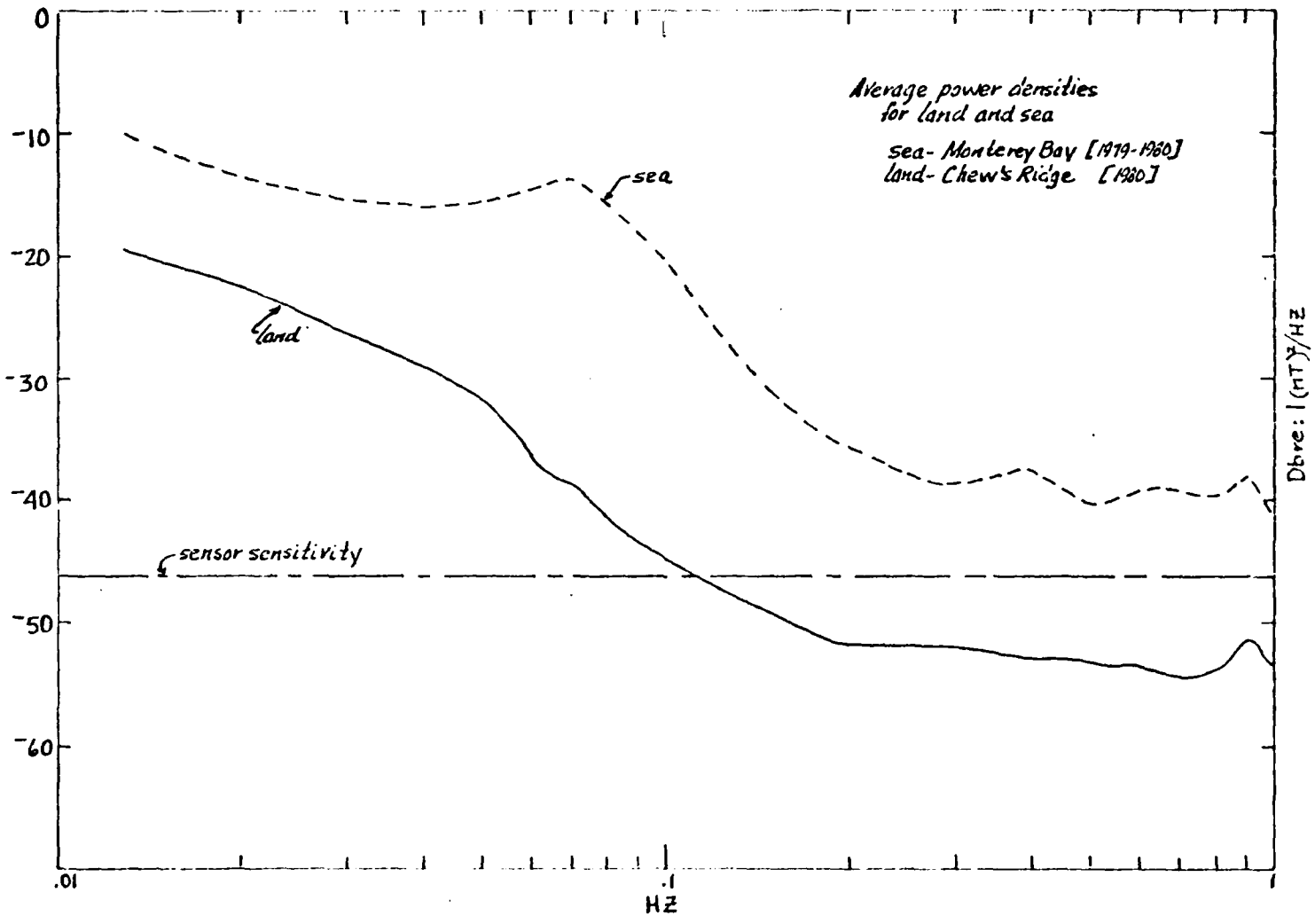
Average power densities
for land and sea
sea- Monterey Bay [1979-1980]
land- Chew's Ridge [1980]
sea
land
sensor sensitivity
0
-10
-20
-30
-40
-50
-60
.01
.1
1
Hz
Dbre: 1 (nT)²/Hz

Figure 15

C. COMPARISON OF NIGHTTIME AND DAYTIME DATA

The curves plotted in Figure 16 represent the average power densitities for the daytime and nighttime data collection periods. They are based on 4 hours during the day covering 2 hours of data collection and 6 observations at night covering 3 hours. The data was all collected at Chew's Ridge over the period 15 August to 19 October, 1980. The nighttime data was weighted by the fact that most was taken during periods of relatively high geomagnetic activity (Figure 14), with most of the data taken on the night of 17-18 October, 1980.

Because of power density falls below the sensor sensitivity at 0.1Hz for the nighttime data, this data was compared only over the 0.0125 to 0.1Hz interval. This interval includes the influences of the Pc 5, Pc 4 and the Pc 2, 3 micropulsations.

The curves in Figure 16 reflect the dominance of the Pc 4 and Pc 3 fluctuations, with a suggestion of the Pc 4 suggested in the data curves, but not quite as prominent due to the averaging process. In this 0.0125 to 0.1Hz interval, the curves are almost parallel with the daytime intensity greater than the night up to 0.06Hz. This suggests that the overall power densities generally conform to the observations of Barry (1979), in that the power density subsides shortly after nightfall.

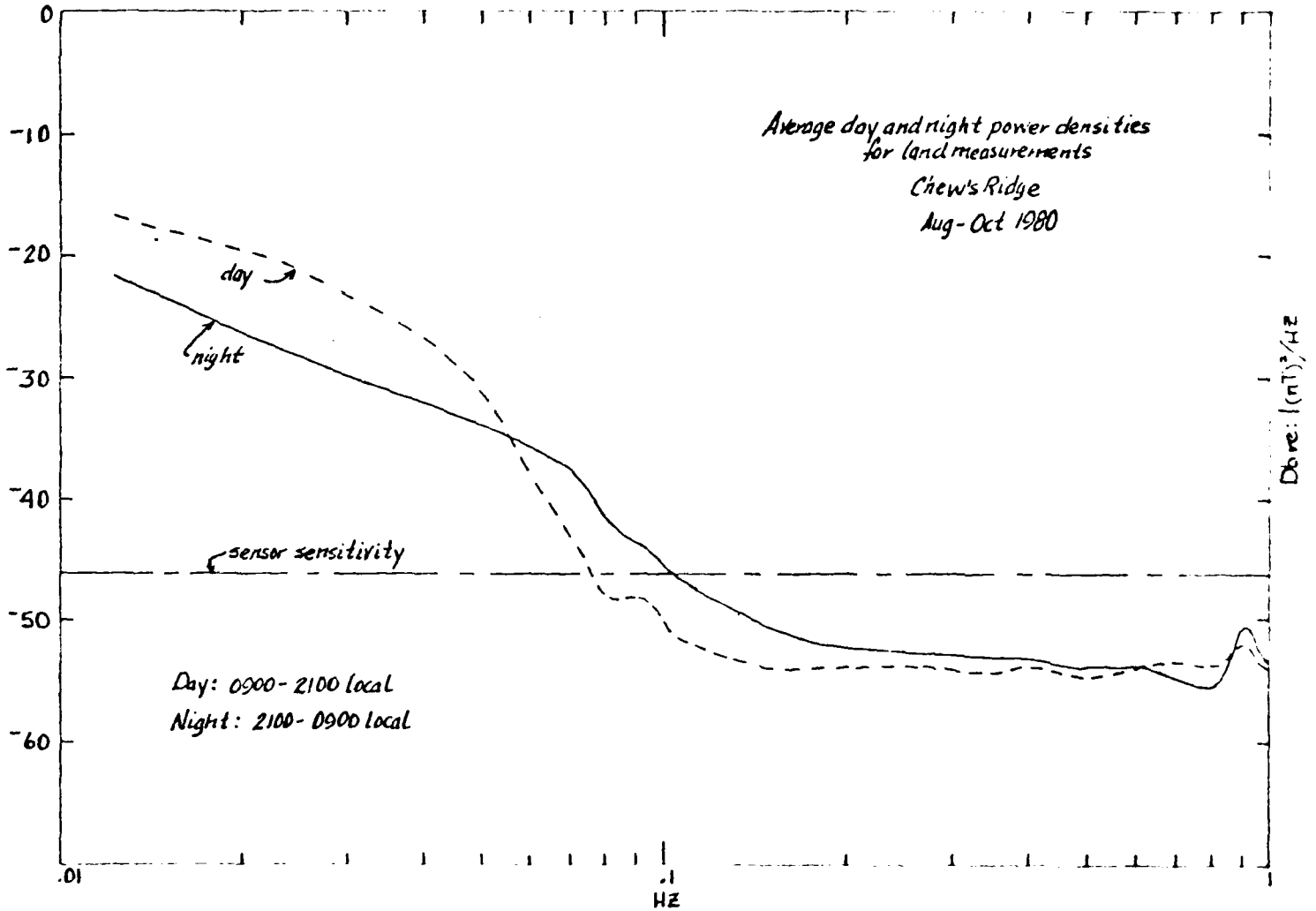
Average day and night power densities
for land measurements
Chew's Ridge
Aug - Oct 1980
day
night
sensor sensitivity
Day: 0900 - 2100 local
Night: 2100 - 0900 local
0
-10
-20
-30
-40
-50
-60
.01
.1
Hz
Db re: 1 (nT)²/Hz

Figure 16

In the Pc 3 region (0.02 to 0.1Hz), an upward shift in the frequency is noted during the transition from day to night. This is due to the increased prominence of the higher frequency Pc 3 pulsations at night. This transition from daytime to nighttime and back was used to define the data collection intervals as day or night. This transition lags local sunrise and sunset by 3 hours, and is accounted for in the data intervals listed (Buxton and Frasier-Smith, 1975). The shift noted in the data correspond to an increased Pc 2 (0.02 to 0.1Hz) activity and shorter period pulsations, also noted by Buxton and Frasier-Smith in 1975.

D. DETECTION OF GEOMAGNETIC FLUCTUATIONS IN ASSOCIATION WITH NUCLEAR TEST DETONATIONS

Underground nuclear testing was scheduled at the Nevada test site for 0800 Pacific Daylight Time on 30 and 31 July, 10 and 17 September, 1980. The Cesium vapor magnetometer system was in place for each of the tests scheduled. None of the tests were executed at the planned times. Because of the limited recording time of the system, any change in the test schedule made it impossible to collect meaningful data.

It was anticipated that some sort of instantaneous fluctuation of the constant field might be observed, although the exact nature of the fluctuation would be difficult to predict. More likely, observable fluctuations would be induced

within the earth's crust. Although the exact mechanism is unknown, piezoelectric interaction of the seismic wave and the crust itself are thought to be the source of the current.

The arrival of the seismic waves can be predicted to an approximate degree. The first wave to arrive would be the compressional, or P wave, which would be relatively small in comparison to the later arriving transverse, or S wave. The last wave to arrive would be the longitudinal, or L wave which travels along the surface of the earth. This would be the largest and most detectable of the seismic waves.

Figure 17 may be used to determine the approximate times of arrival of these waves by entering the graph with the approximate value of Omega. Omega is the angle formed by the sensing station, the center of the earth, and the point of the seismic disturbance. In the case of the Nevada tests, 837 miles was used as the distance between the nuclear test site and the magnetometer, and 3960 miles for the radius of the earth, to calculate the approximate value for omega. The following relationship was used to determine this value:

$\cos \gamma = (a^2 + b^2 - c^2) \div 2ab$, where:

c = distance between the test site and the observer

$a=b$= radius of the earth

The calculation, using the values noted, produced a value

[Adapted from Gordon,1972]

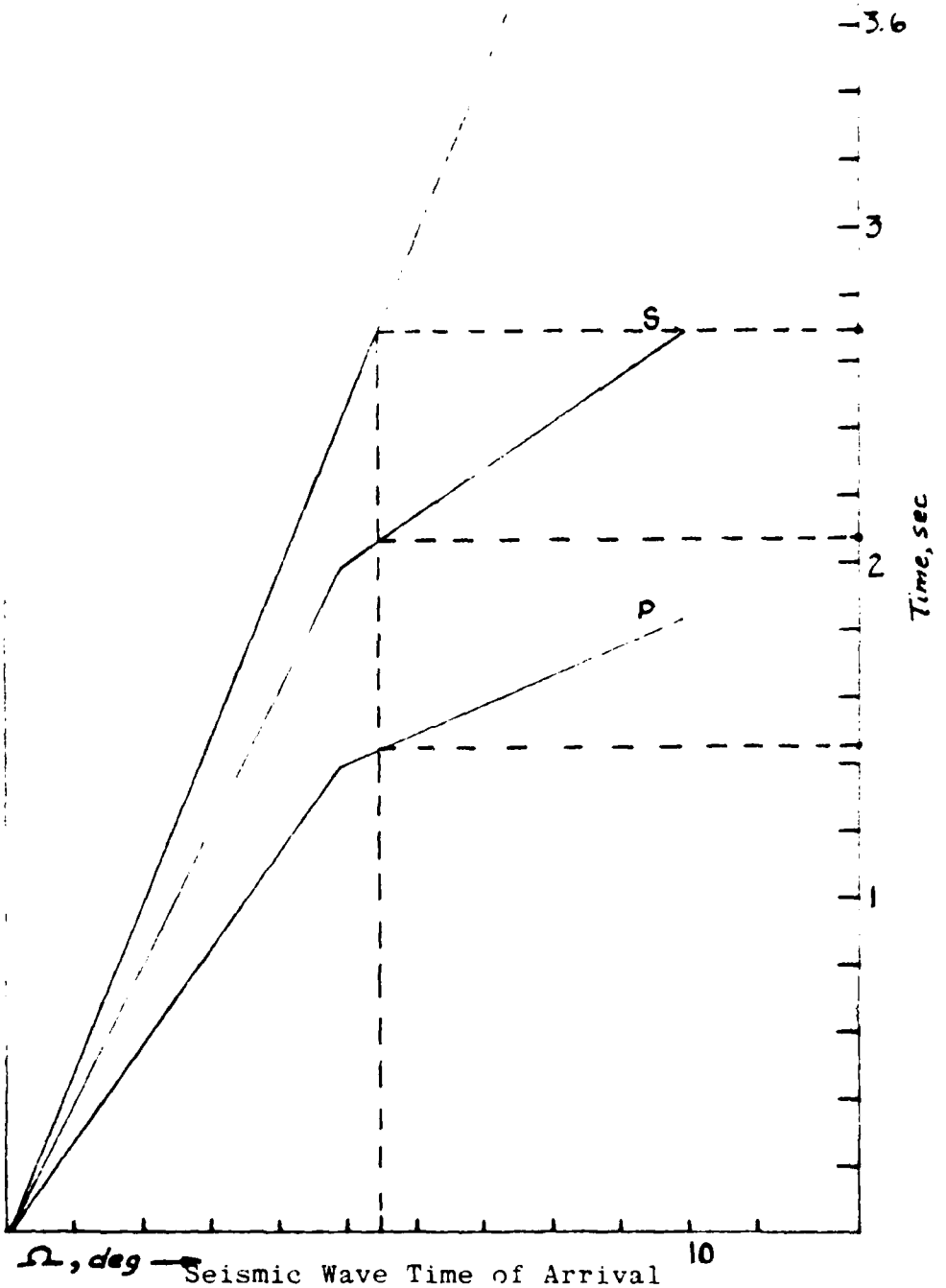

Seismic Wave Time of Arrival

Figure 17

for omega of 5.4 degrees. With this value, Figure 17 can be entered and the arrival times of the respective seismic waves read on the vertical scale.

Atmospheric detonations of nuclear devices are rare and adequate notification of the exact times of such tests is difficult to obtain due to the extreme sensitivity of the information. An atmospheric test was conducted by the Peoples Republic of China on the 15th of October, 1980. Unfortunately, data was collected in a time frame prior to the test, so that the transient effects of the blast could not be seen. Balser and Wagner (1963) observed the pulsations generated by a United States atmospheric test in 1962, and compared them with pulses that were diurnal in nature. Figure 18 is a real time trace of a typically active day, and shows irregular noise spikes. These spikes are similar to those observed by Balser and Wagner 2 seconds after detonation. It would be difficult to distinguish a nuclear detonation from naturally induced magnetospheric phenomena, unless the actual test were in some way anticipated.

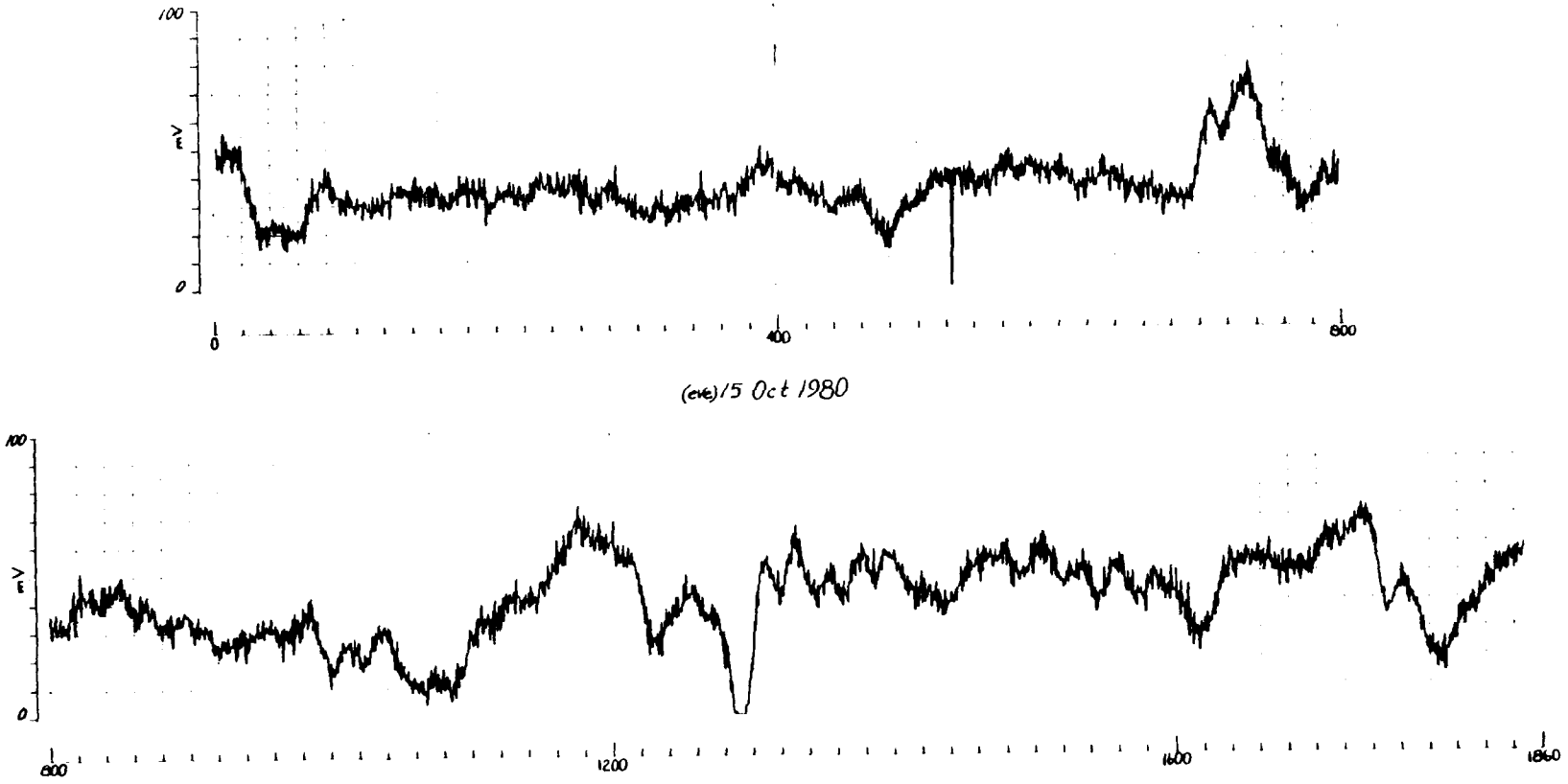

Real Time Display of Geomagnetic Fluctuations

Figure 18

V. RECOMMENDATIONS

The sea and land configurations of the Cesium vapor magnetometer system have proven themselves capable of detecting low frequency geomagnetic fluctuations in the frequency range of interest. The system presently in use is simple and straight forward in operation, with potential for future interfacing with more sophisticated data recording techniques. The overriding difficulty in adapting the Cesium vapor magnetometer system to larger volume data collection methods (on the order of days or weeks) is the limiting factor of power consumption. Although the land version of the system can be serviced on a regular basis, the underwater system configuration does not permit regular access to replace the batteries in the system. Until this obstacle can be overcome, the longest period of operation is 36 hours, assuming the frequency to voltage discriminator is powered by 18 amp-hour Gelyte batteries. In the case of the 2.6 amp-hour batteries, the operating time would be much less, and depend on the temperature of the operating environment.

There is a need for some method of accurately recording the orientation of the sensor on the sea floor, particularly if the sensor is the component reading type (coil or superconducting magnetometers). The primary difficulty is the

directional recording device must not affect the operation of the sensor. Some sort of bubble type level, in a liquid that will freeze the bubble in position after a certain time in the cold sea water would be suitable.

Simultaneous data collection capability is highly desireable to allow direct correlation of the spectra from several locations. Such a set-up will allow the study of land, sea and deep sea fluctuations and lead to a more complete understanding of the sea water and sea floor contribution to the observed power spectra. An accurate clock is required to impose some timing signal on the tapes to allow exact time correlation.

The information gained from the analysis of the power spectra can be used to make some predictions in regard to geomagnetic activity. The understanding of the sea water and sea floor contributions can be used in conjunction with current military magnetic sensing devices. Hopefully, some sort of index can be developed that will allow sensor operators to set equipment sensitivities to best mask the background effects of active days and thereby enhance detection probability.

APPENDIX A

A. DATA COLLECTION EQUIPMENT

1. Cesium vapor magnetometer, Varian Associates Model 4938

Characteristics

Power Required:	28-32V dc
Sensitivity:	5×10^{-12} tesla
Range:	Continuous from 20,000 to 80,000 nT
Proportionality Constant:	3.499 Hz/nT
Output:	176.5 KHz, 0.2 volt peak to peak

Operation: The magnetometer acts as an oscillator whose frequency, (Larmour Frequency) is proportional to the intensity of the magnetic field. This proportionality is caused by the effect of the magnetic field on the Zeeman splitting of the energy levels of the Cesium valence electron. The separation of the energy levels must be equal to the energy of emitted or absorbed photons. The energy is equal to Planck's constant times the frequency, $E = h\nu$. The energy difference between levels E is directly proportional to the local magnetic field:

Operation: The 2 KHz sine wave output is fed into one channel of the cassette recorder.

4. 2 Channel Analog Cassette Recorder (Marantz Model DC-330)

Characteristics

Power Required:	6V dc
Tape Speed:	1 7/8 inches/second
Frequency Range:	40Hz to 12 KHz
Wow and Flutter:	.12%

Operation: The VCO output and 2 KHz reference oscillator are placed on cassette tape. Care must be taken to have the input levels balanced for more efficient mixing during data reduction. The speaker monitor should be turned off during data collection to increase battery life.

There are two methods of delaying recording until the system is clear of the launching vessel, a pressure sensitive switch or a timer. Of the two methods, a timer is preferred so as to control the exact time of data collection.

5. Frequency to Voltage Discriminator (Anadex Model PI-375)

Characteristics

Power Required:	22-30V dc
Input Frequency:	5 to 2000Hz
Output Voltage:	0-5V full scale

Operation: The sensor coupler output is converted to a dc voltage, the conversion is 2.5 mv/nT.

$$E = \frac{g\ e\ h}{4\ \pi\ m} B$$

g = Lande "g factor"

e = charge on an electron

h = Planck's constant

m = electron mass

B = magnetic field strength

By measuring ν, the field intensity B can thereby be determined. The output frequency is transmitted along a coaxial cable to the sensor coupler.

2. Sensor Coupler (Varian Associates Model 4938)

Characteristics

Power Required:	28-32V dc (powers both the sensor and sensor coupler)
Output:	1500Hz square wave, 5V peak to peak

Operation: The sensor coupler provides power to the sensor, and receives the Larmour Frequency output via the same coaxial cable. The sensor output is mixed with an appropriate crystal oscillator to produce a 0-2000Hz square wave (1500Hz nominal). The coupler also has an oven to keep the crystal at a constant 75°C for stable output.

3. 2 KHz Reference Oscillator

Characteristics

Power Required:	6V dc
Output:	2 KHz sine wave

The discriminator has an internal low pass filter which begins to cut off at 10Hz, falling off at 24 dB per decade. The output is then fed into a voltage controlled oscillator.

6. Voltage Controlled Oscillator

Characteristics

Power Required:	±6V dc
Output:	Centered at 1.5 KHz
Variation:	122Hz/nT

Operation: The output of the Discriminator is fed into the VCO where A-C coupling occurs in the preamplifier stage. The purpose of this coupling is to prevent the high amplitude ELF (less than .1Hz) signals from overdriving the data collection system. The VCO output is fed into the second channel of the tape recorder.

7. Power Supplies (Gould Gelyte Batteries)

Three battery types are used in the system:

2 - 12 volt 18 amp-hour

2 - 6 volt 18 amp-hour

1 - ±6 volt 2.6 amp-hour

2 - 12 volt 2.6 amp-hour

The Gould sealed gel electrolyte, rechargeable batteries have proven to be quite reliable and efficient sources of power. Their life can be extended by careful charging (1 amp for the 18 amp-hour batteries, .2 amp for the 2.6 amp-hour

batteries). It must be noted however, that the batteries are the limiting factor in the length of time the system can be deployed. Operations at Chew's Ridge showed that battery life shortens at low temperatures (< 35°F). This is another consideration which limits the amount of time available for data collection.

B. DATA REDUCTION EQUIPMENT

As shown in Figure 6, the data reduction system uses the same basic components of the collection system, with the exception of a mixer, and an amplifier to provide a large enough signal to drive the discriminator. The discriminator output is fed into a variable amplifier, which is required to adjust the signal DC level. Without this DC bias, the discriminator output might overload the spectrum analyzer and adversely affect the averaging process.

C. COLLECTION SYSTEM TEST PROCEDURE

The following procedures are recommended to ensure proper system operation prior to leaving the laboratory.

Power Supplies: Voltage should be checked on all batteries prior to use. A battery log would be helpful to record amount of charge and charge rate.

Sensor: The simplest test of sensor operation is to provide power to the sensor (via the sensor coupler) and checking

to see that current is being drawn by observing the "sensor current" meter on the coupler.

Sensor Coupler: The sensor coupler operation is easily checked by first observing the green power on light once 30V dc is placed on the coupler. Proper mixing can be checked placing the mixer output voltage on an oscilliscope. Figure 7 of the Varian Associates' handbook shows the expected waveform.

VCO: After applying power, and with no input, examine frequency output of the VCO, 1500Hz at 6V is the expected value.

Proper operation of the discriminator is best checked by using a synthetic source to duplicate a frequency modulated Larmour Frequency and run a check on the full system. To accomplish this, the following test equipment is required:

A signal is generated to simulate the Larmour output of the sensor:

FM GENERATOR 176.5 KHz 0.1 to 0.2V pp

AM GENERATOR 1Hz SINE WAVE, (level adjusted so as not to overdrive system).

This input is placed at the Larmour output jack on the sensor coupler. The mixer output is then fed through the system as described in Figure 6. This also serves as an operatability check for the entire system.

APPENDIX B

This is a compilation of the individual data curves for both land and sea observations recorded over the period 21 July, 1980 to 19 October, 1980. The data was analyzed in two different bandwidths, 0-5Hz (Figures 19 to 34) for all data observations and 0-1Hz (Figures 35 to 38) for selected data runs.

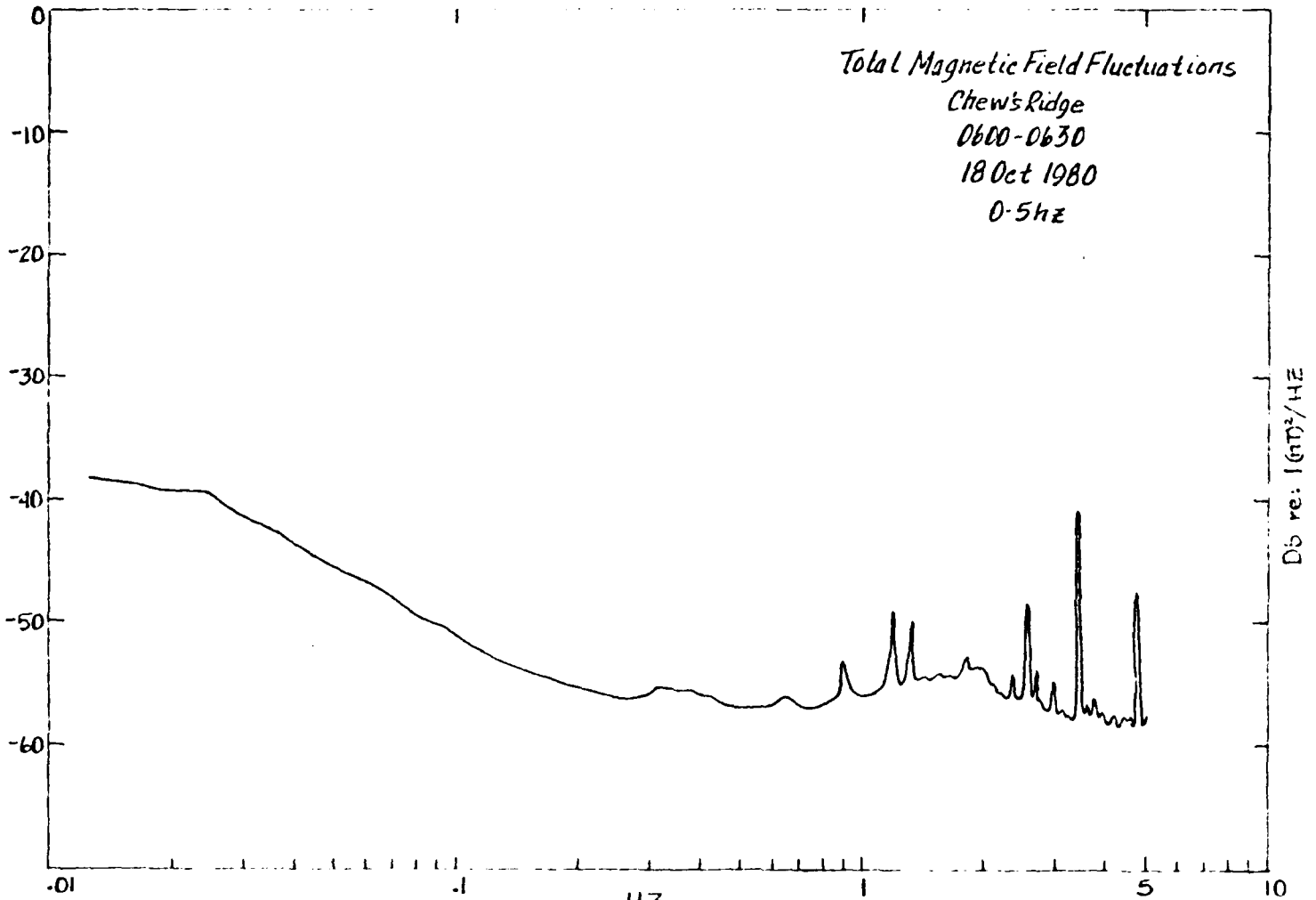
Total Magnetic Field Fluctuations
Chew's Ridge
0600-0630
18 Oct 1980
0-5hz
0
-10
-20
-30
-40
-50
-60
Db re: 1(nT)²/HZ
.01
.1
1
5
10
HZ
Figure 19

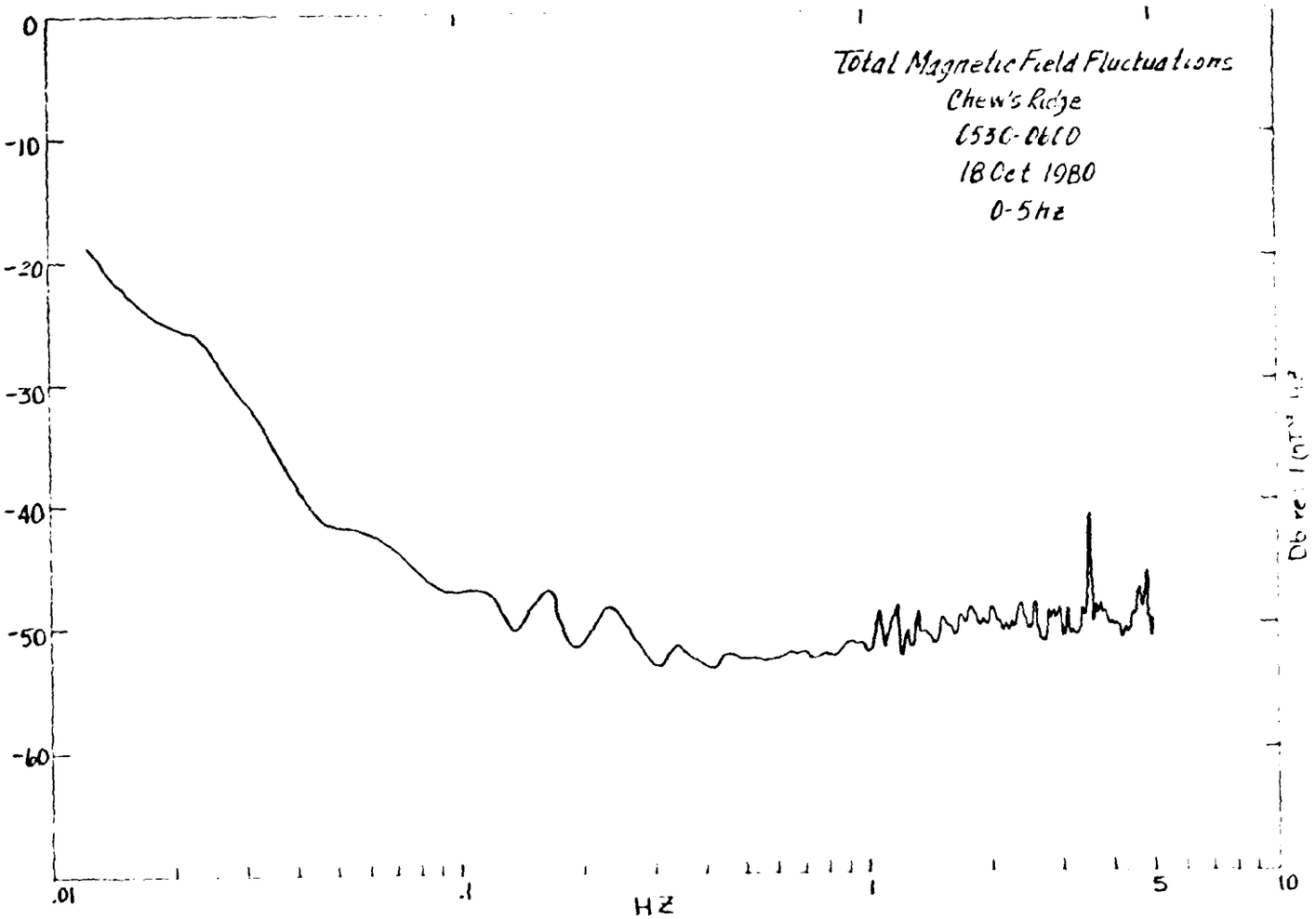
Total Magnetic Field Fluctuations
Chew's Ridge
0530-0610
18 Oct 1980
0-5 Hz
0
-10
-20
-30
-40
-50
-60
.01
.1
1
5
10
HZ
Db re 1 (nT)²

Figure 20

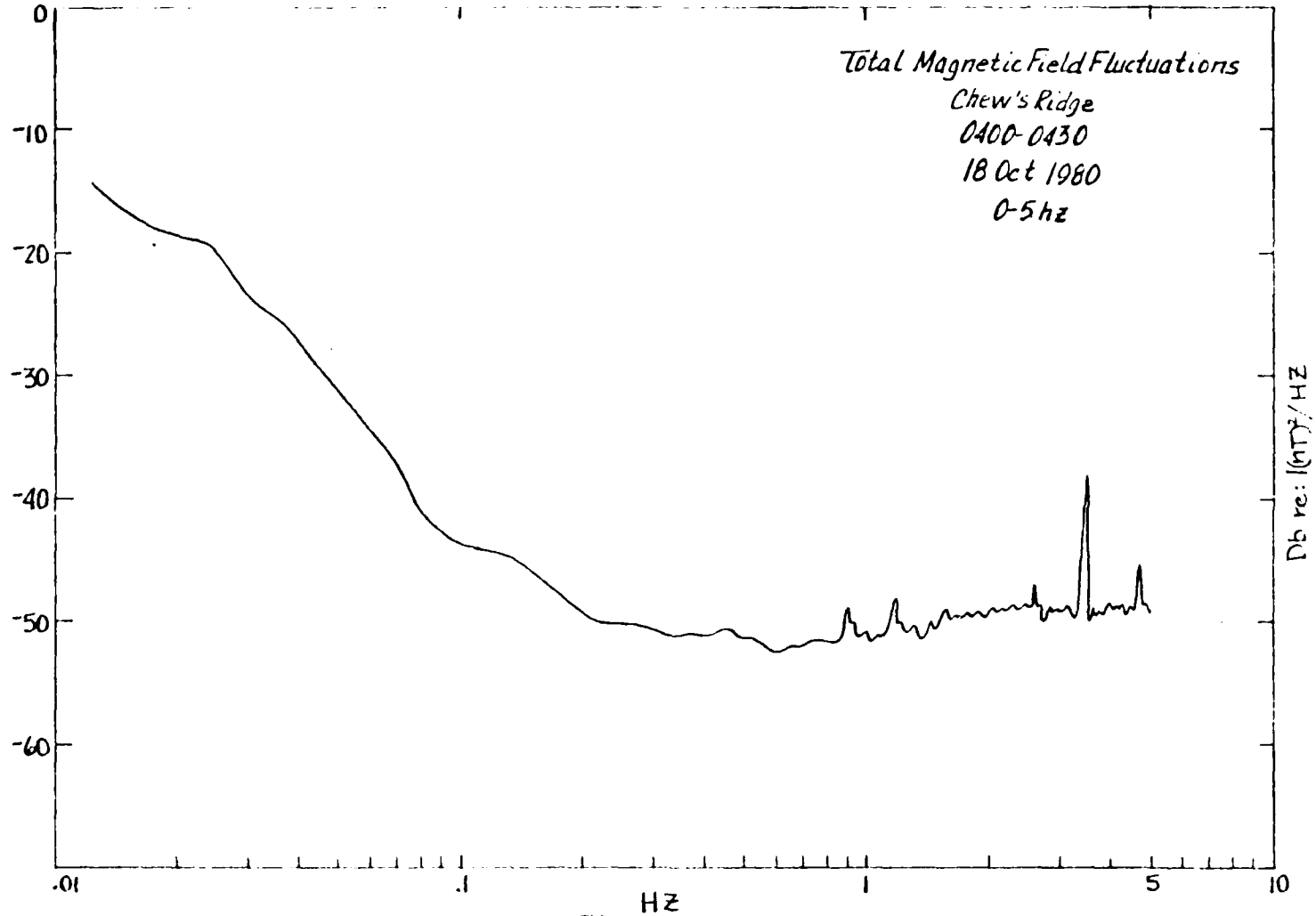
Total Magnetic Field Fluctuations
Chew's Ridge
0400-0430
18 Oct 1980
0-5hz
0
-10
-20
-30
-40
-50
-60
.01
.1
1
5
10
Hz
Db re: 1(nT)²/Hz

Figure 21

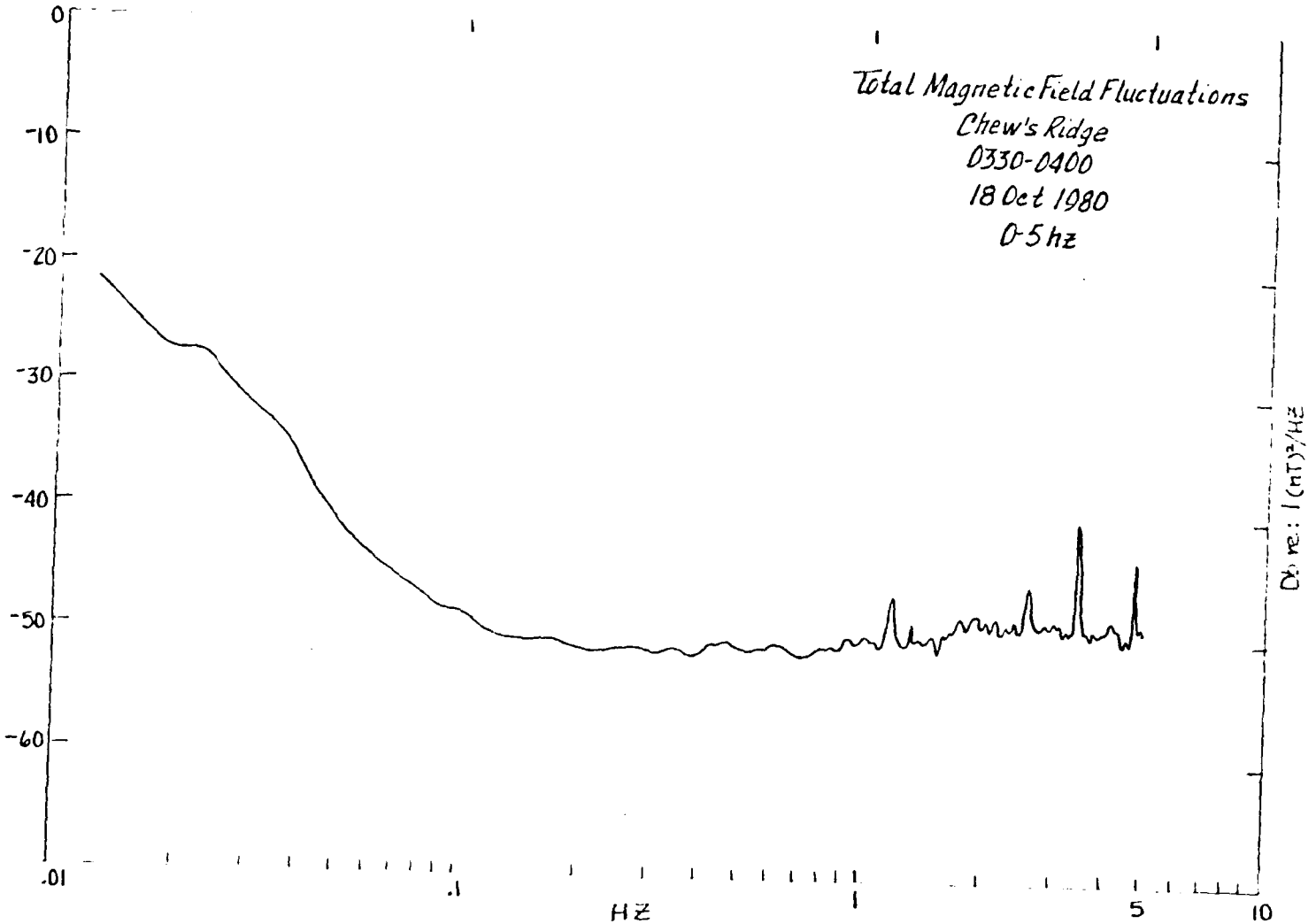
Total Magnetic Field Fluctuations
Chew's Ridge
0330-0400
18 Oct 1980
0-5 hz
0
-10
-20
-30
-40
-50
-60
.01
.1
1
5
10
HZ
DB re: 1 (nT)²/HZ

Figure 22

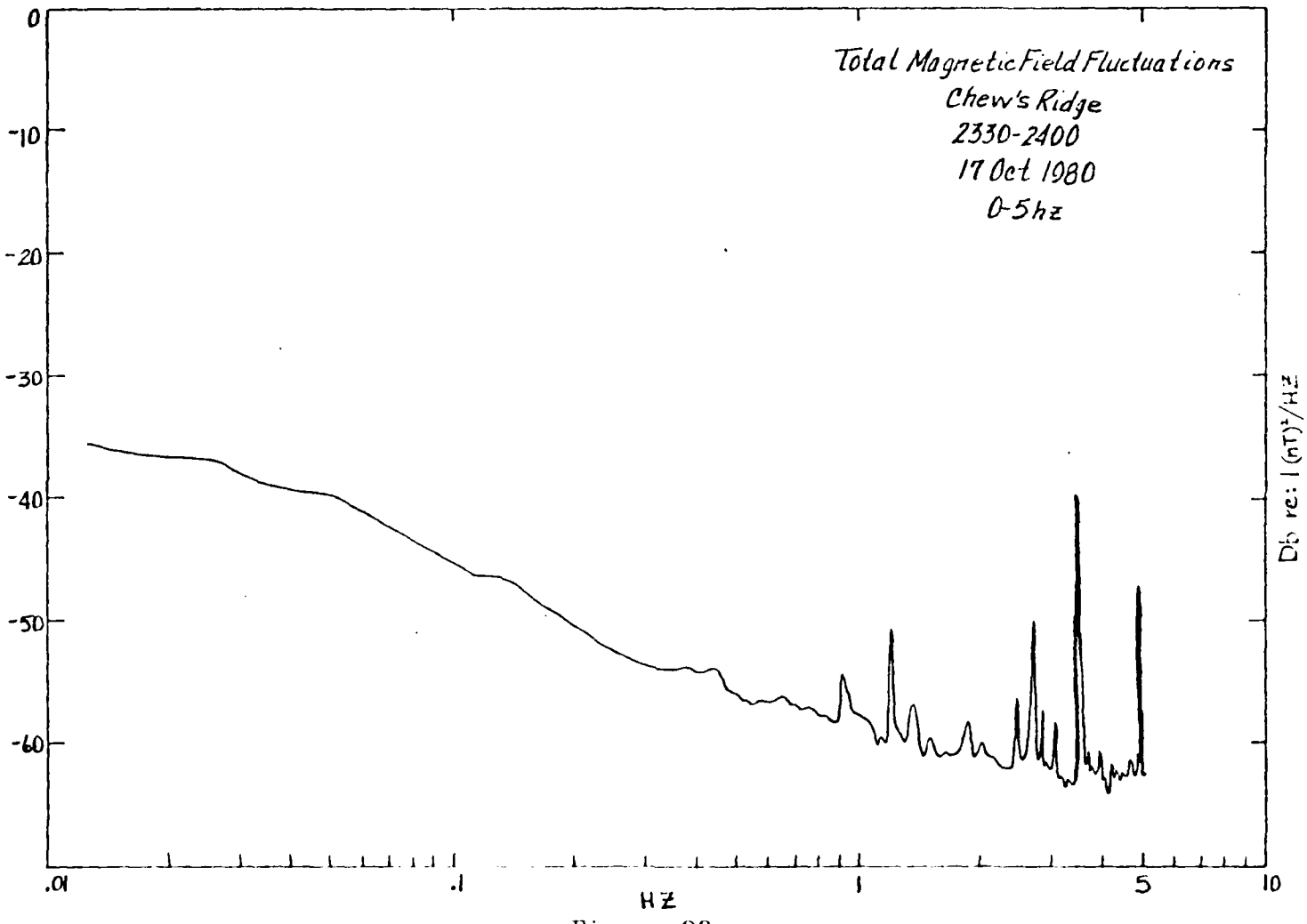
Total Magnetic Field Fluctuations
Chew's Ridge
2330-2400
17 Oct 1980
0-5hz
0
-10
-20
-30
-40
-50
-60
.01
.1
1
5
10
HZ
Db re: 1 (nT)²/HZ

Figure 23

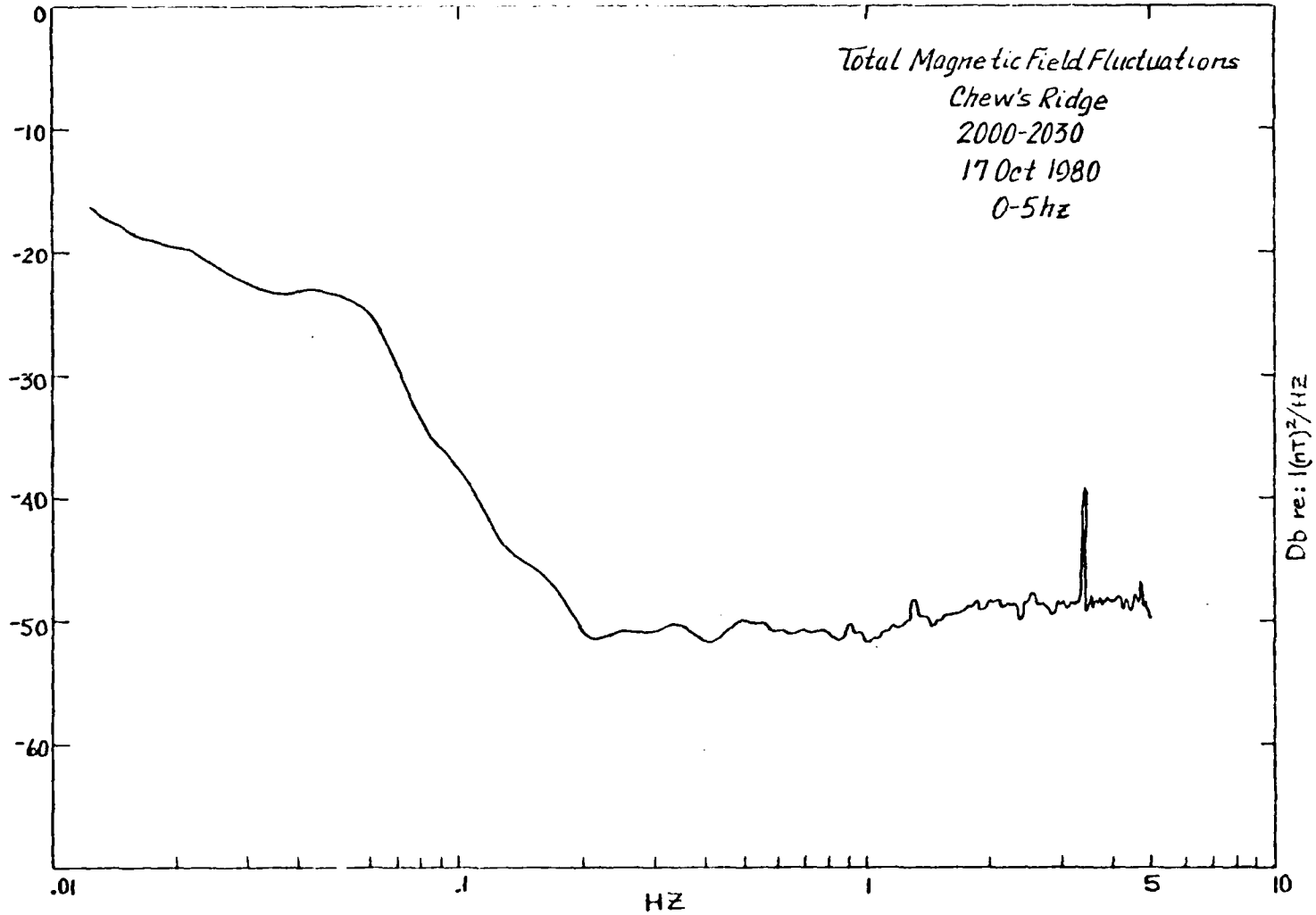
Total Magnetic Field Fluctuations
Chew's Ridge
2000-2030
17 Oct 1980
0-5hz
0
-10
-20
-30
-40
-50
-60
.01
.1
1
5
10
HZ
Db re: 1(nT)²/HZ

Figure 24

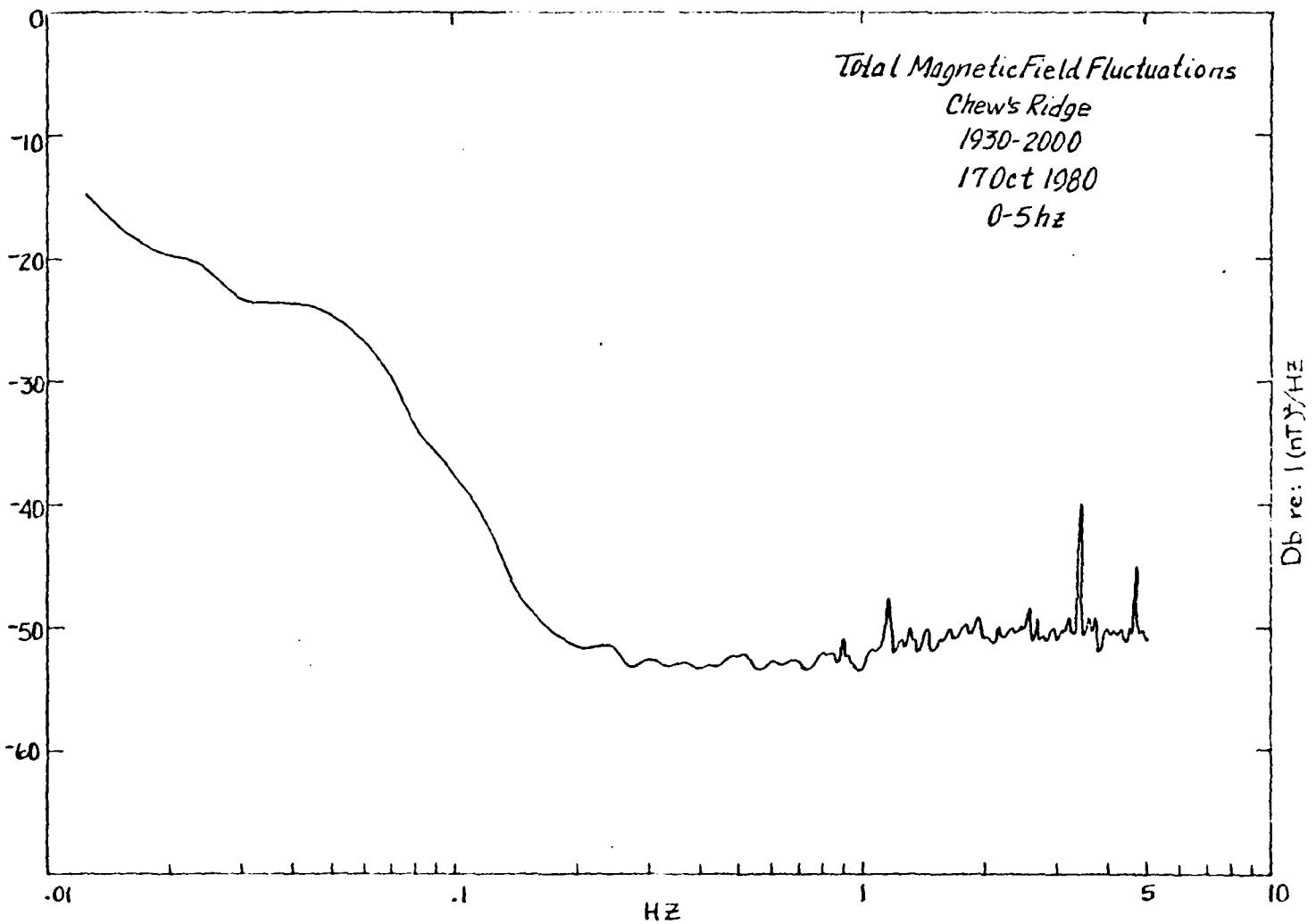
Total Magnetic Field Fluctuations
Chew's Ridge
1930-2000
17 Oct 1980
0-5 hz
0
-10
-20
-30
-40
-50
-60
Db re: 1 (nT)²/Hz
.01
.1
1
5
10
HZ

Figure 25

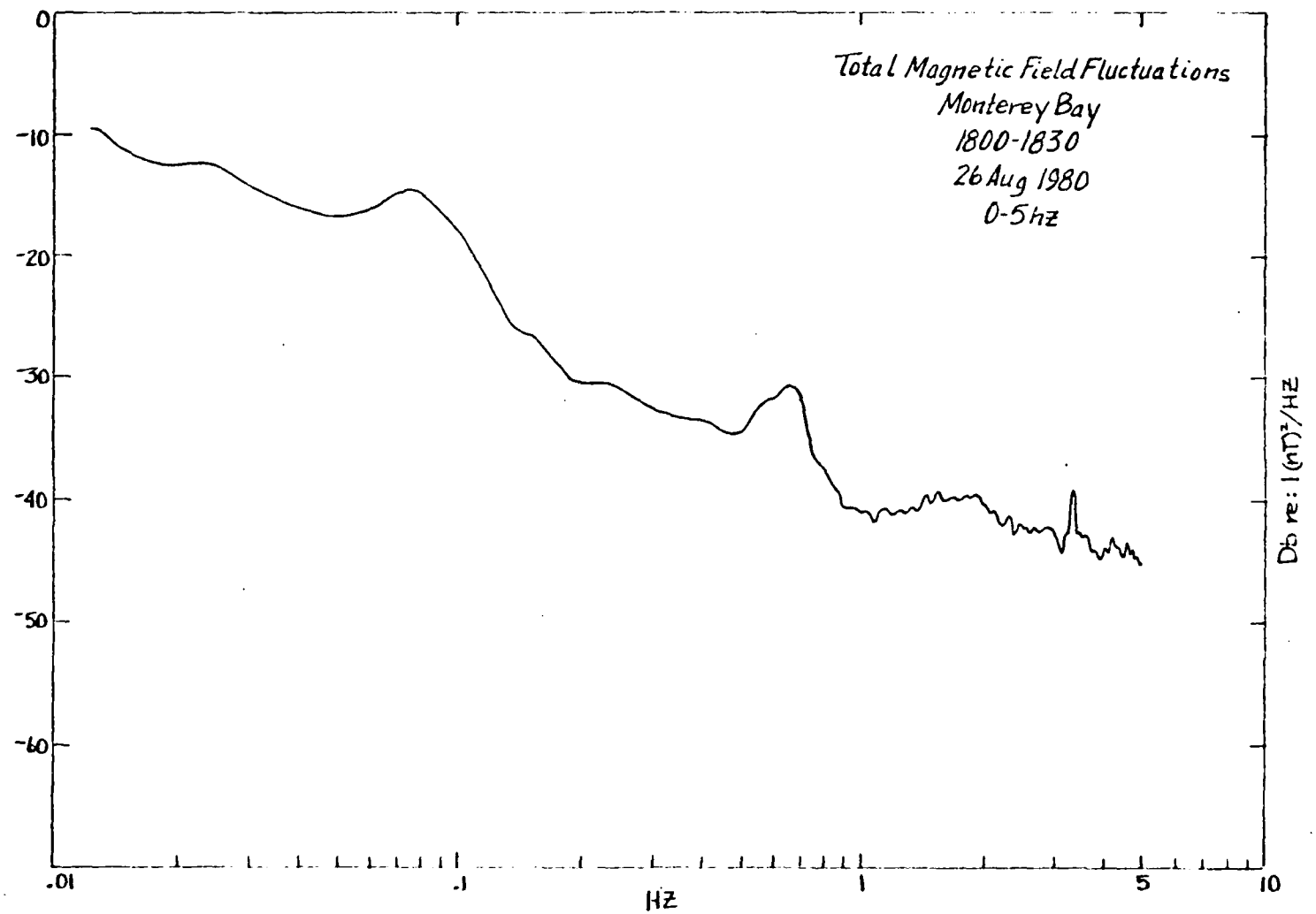
Total Magnetic Field Fluctuations
Monterey Bay
1800-1830
26 Aug 1980
0-5 hz
0
-10
-20
-30
-40
-50
-60
.01
.1
1
5
10
HZ
Db re: 1 (nT)²/HZ

Figure 26

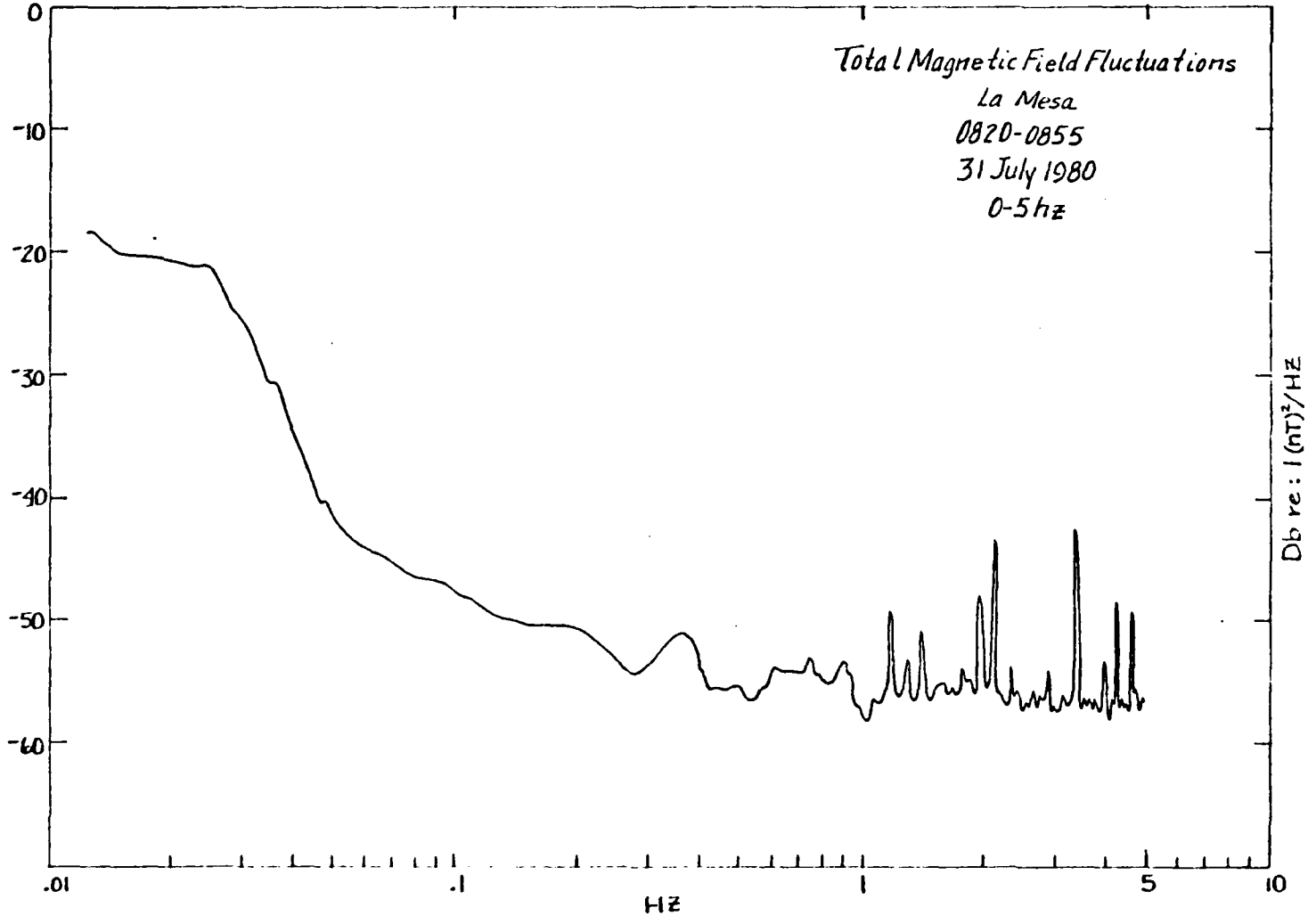
Total Magnetic Field Fluctuations
La Mesa
0820-0855
31 July 1980
0-5 hz
0
-10
-20
-30
-40
-50
-60
.01
.1
1
5
10
Hz
Db re: 1 (nT)²/Hz

Figure 27

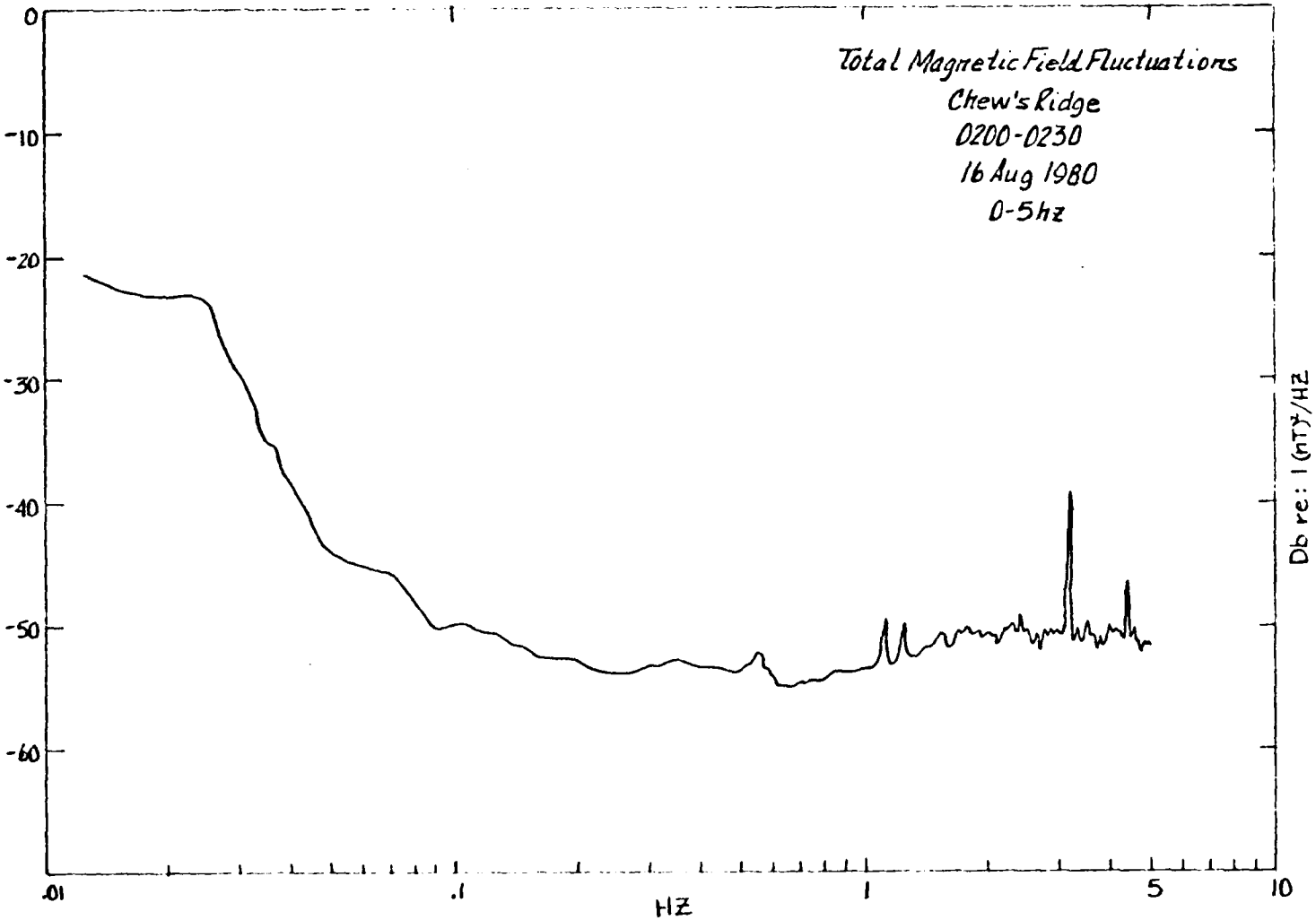
Total Magnetic Field Fluctuations
Chew's Ridge
0200-0230
16 Aug 1980
0-5hz
0
-10
-20
-30
-40
-50
-60
.01
.1
1
5
10
HZ
Db re: 1 (nT)²/HZ

Figure 28

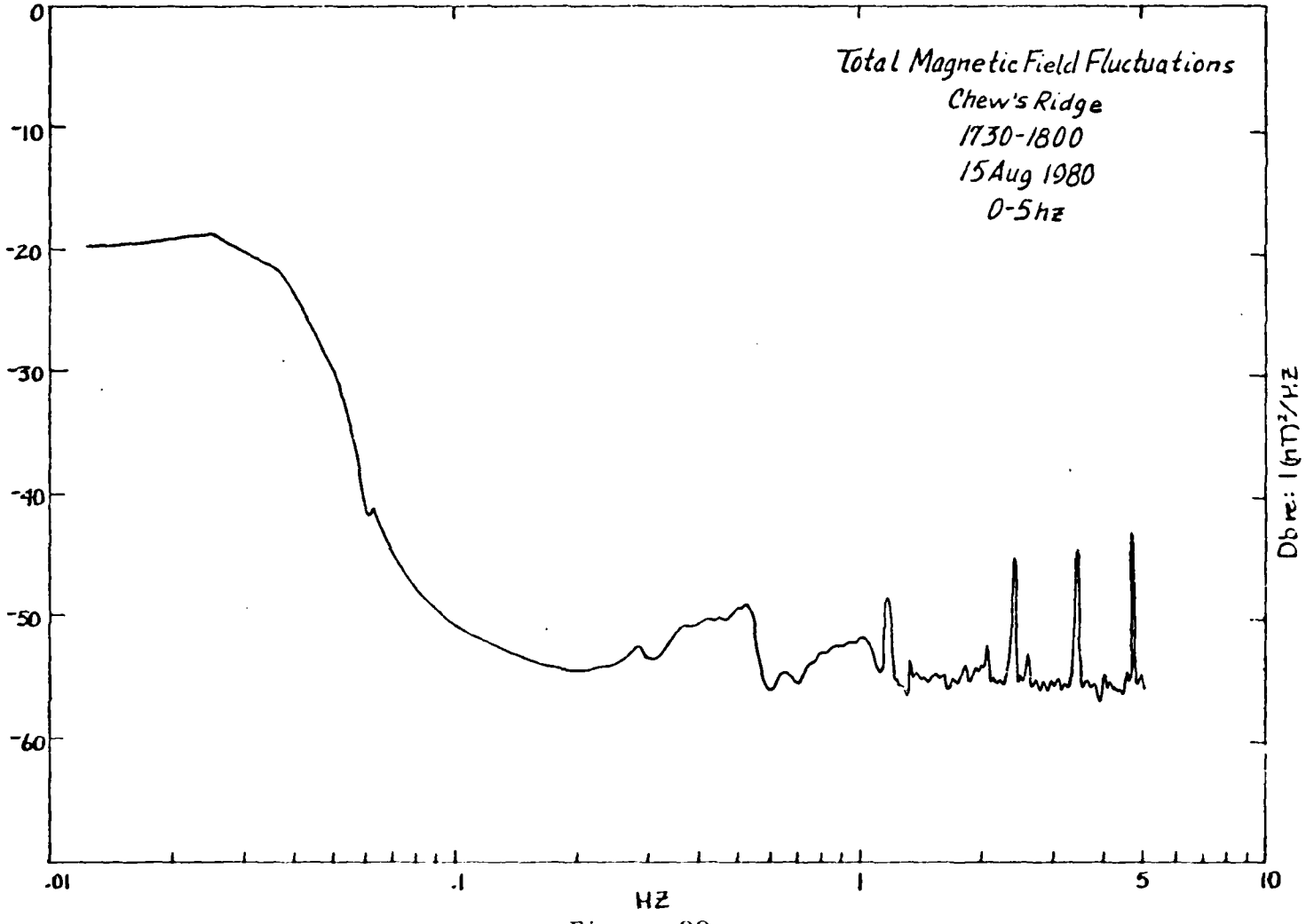
Total Magnetic Field Fluctuations
Chew's Ridge
1730-1800
15 Aug 1980
0-5hz
0
-10
-20
-30
-40
-50
-60
.01
.1
1
5
10
HZ
Db re: 1(nT)²/Hz

Figure 29

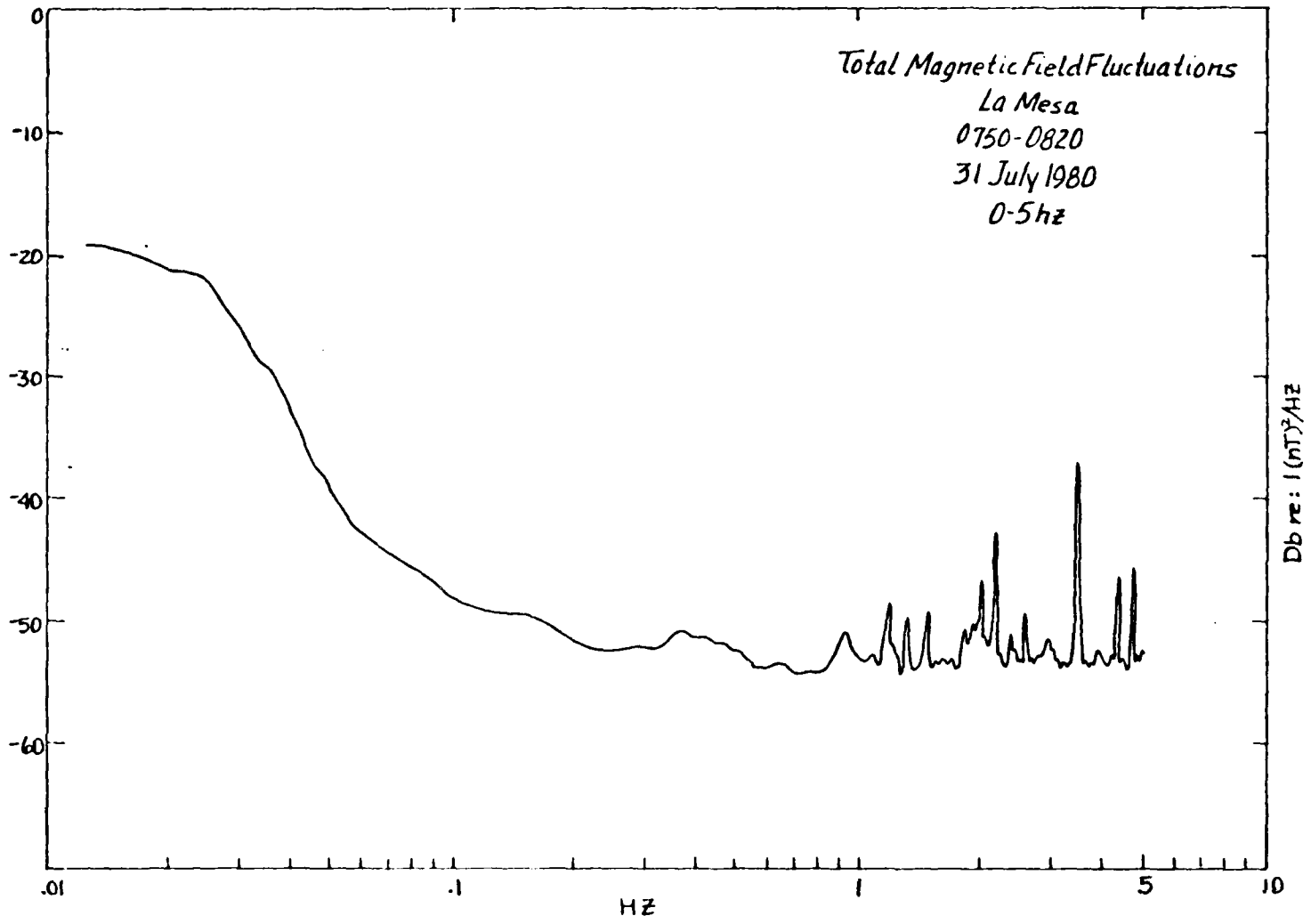
Total Magnetic Field Fluctuations
La Mesa
0750-0820
31 July 1980
0-5hz
0
-10
-20
-30
-40
-50
-60
.01
.1
1
5
10
Hz
Db re: 1 (nT)²/Hz

Figure 30

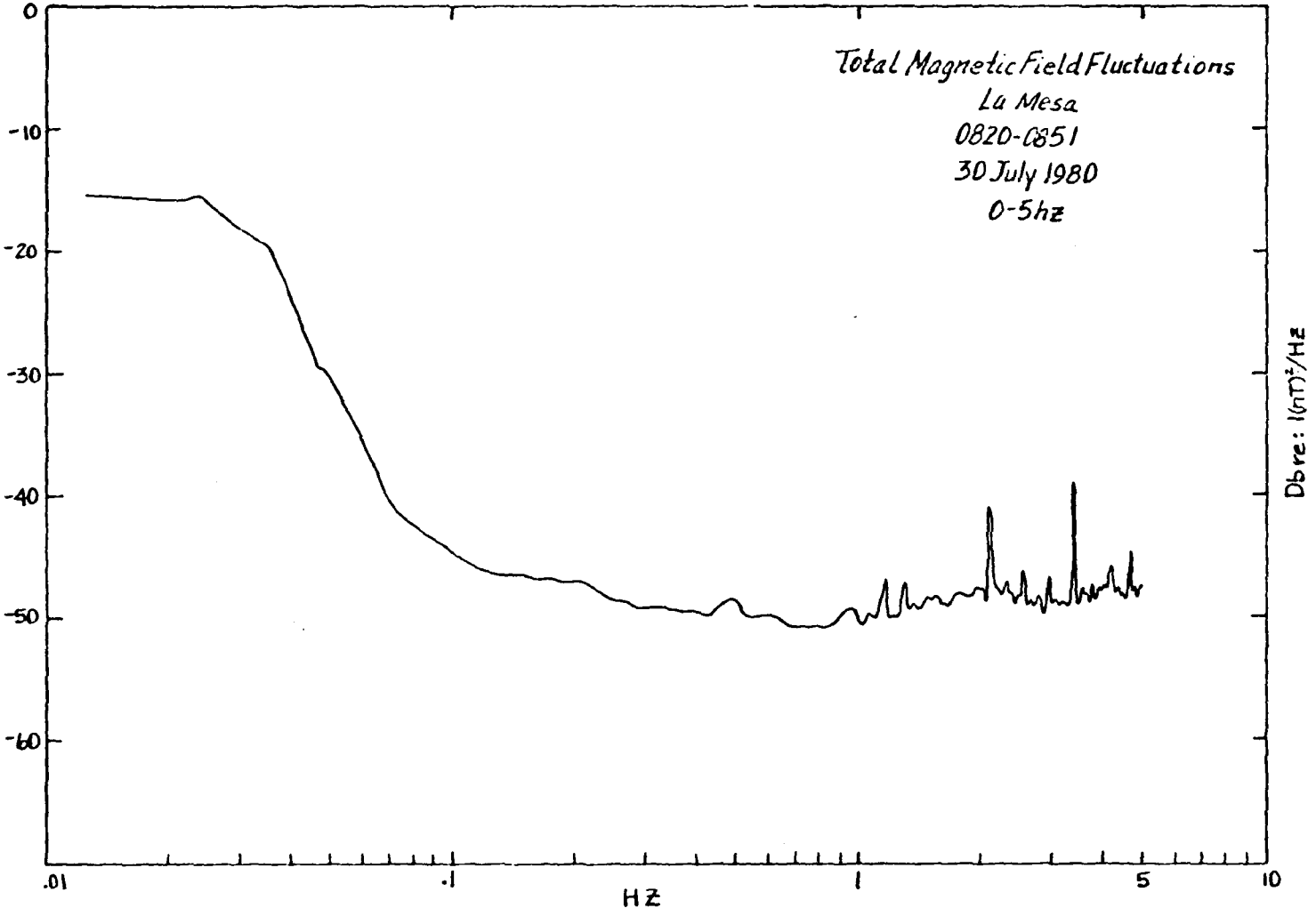
Total Magnetic Field Fluctuations
La Mesa
0820-0851
30 July 1980
0-5hz
0
-10
-20
-30
-40
-50
-60
.01
.1
1
5
10
Hz
Dbre: 1(nT)²/Hz

Figure 31

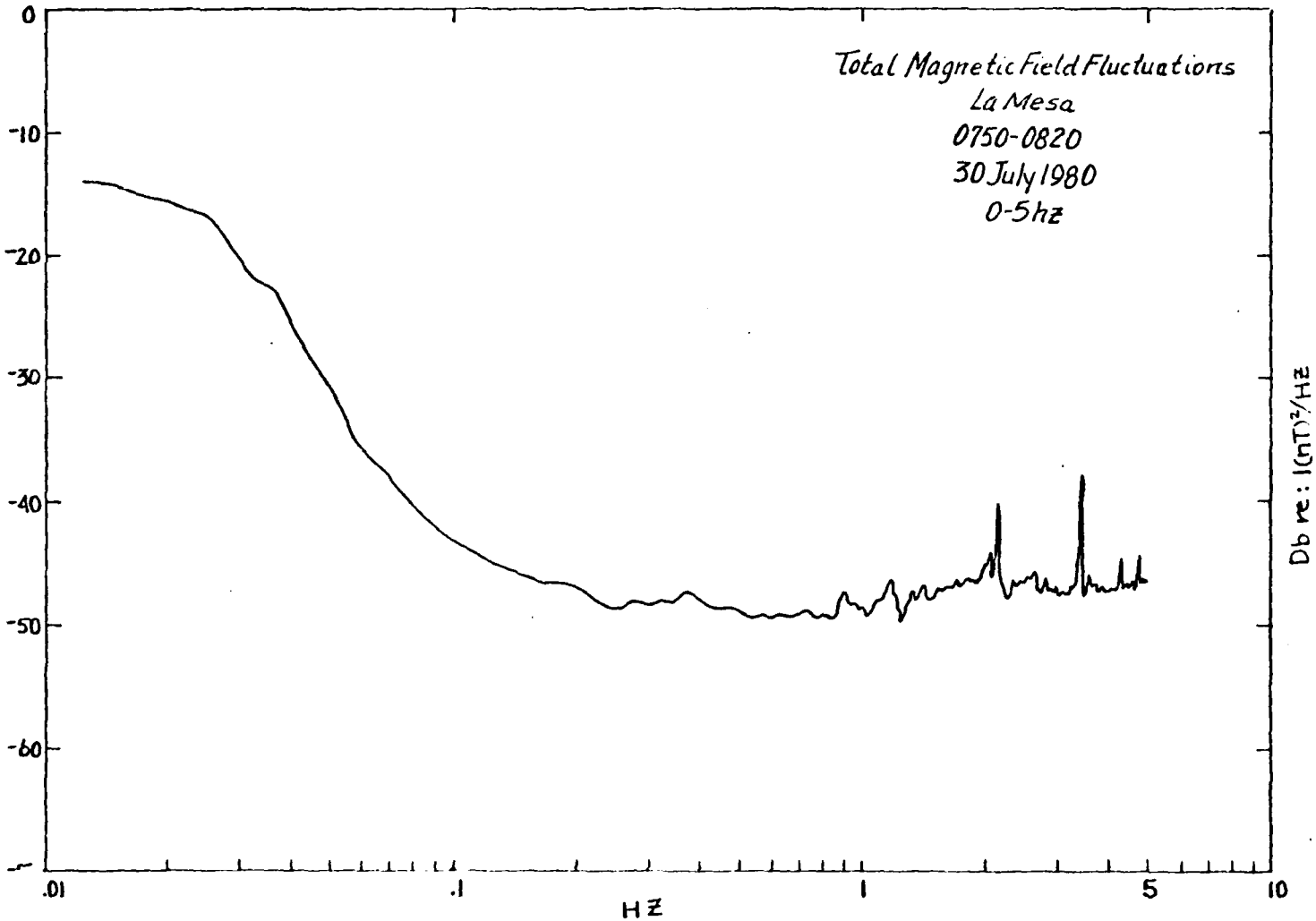
Total Magnetic Field Fluctuations
La Mesa
0750-0820
30 July 1980
0-5hz
0
-10
-20
-30
-40
-50
-60
.01
.1
1
5
10
HZ
Db re: 1(nT)²/Hz

Figure 32

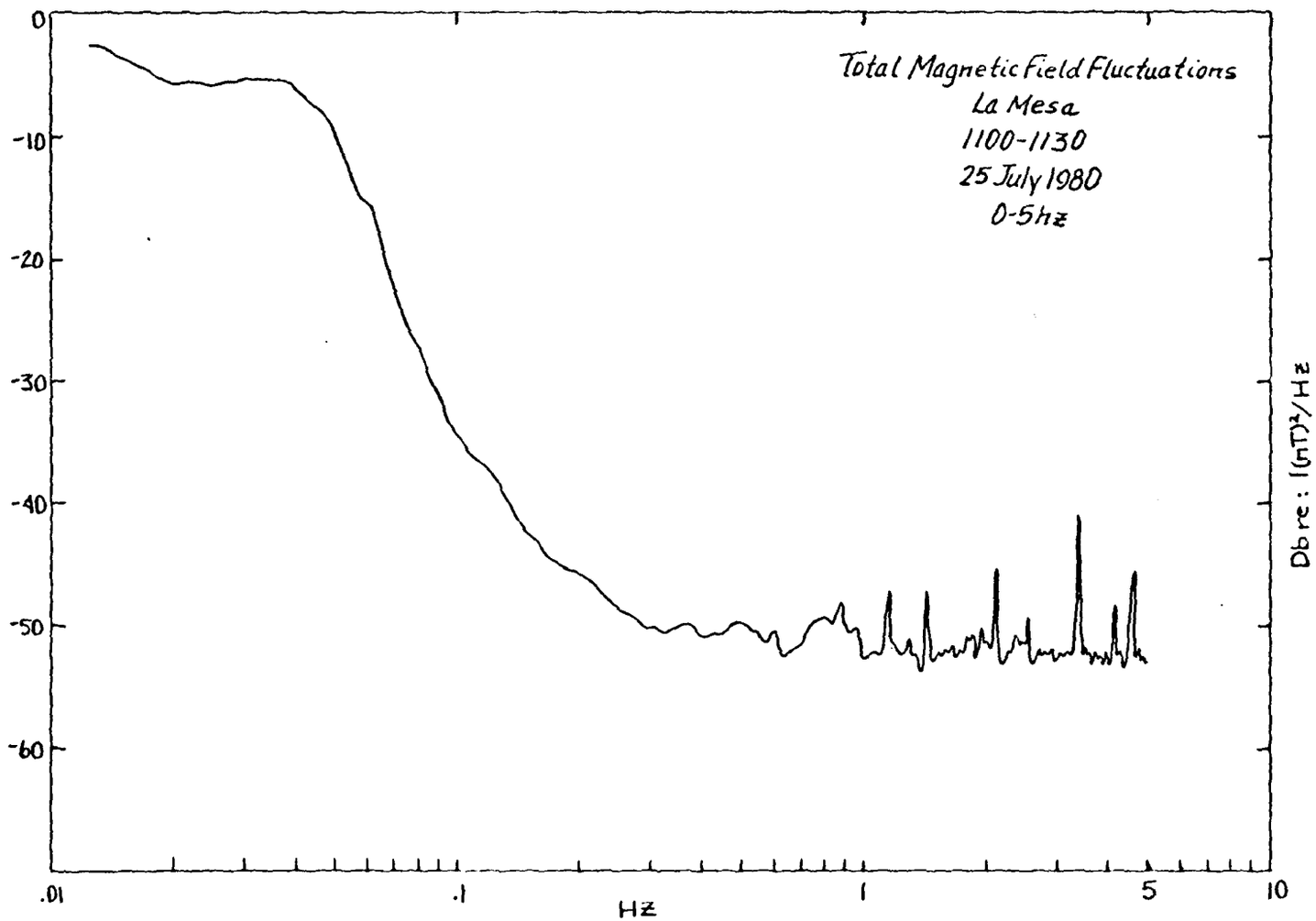
Total Magnetic Field Fluctuations
La Mesa
1100-1130
25 July 1980
0-5hz
0
-10
-20
-30
-40
-50
-60
.01
.1
1
5
10
Hz
Db re: 1(nT)²/Hz

Figure 33

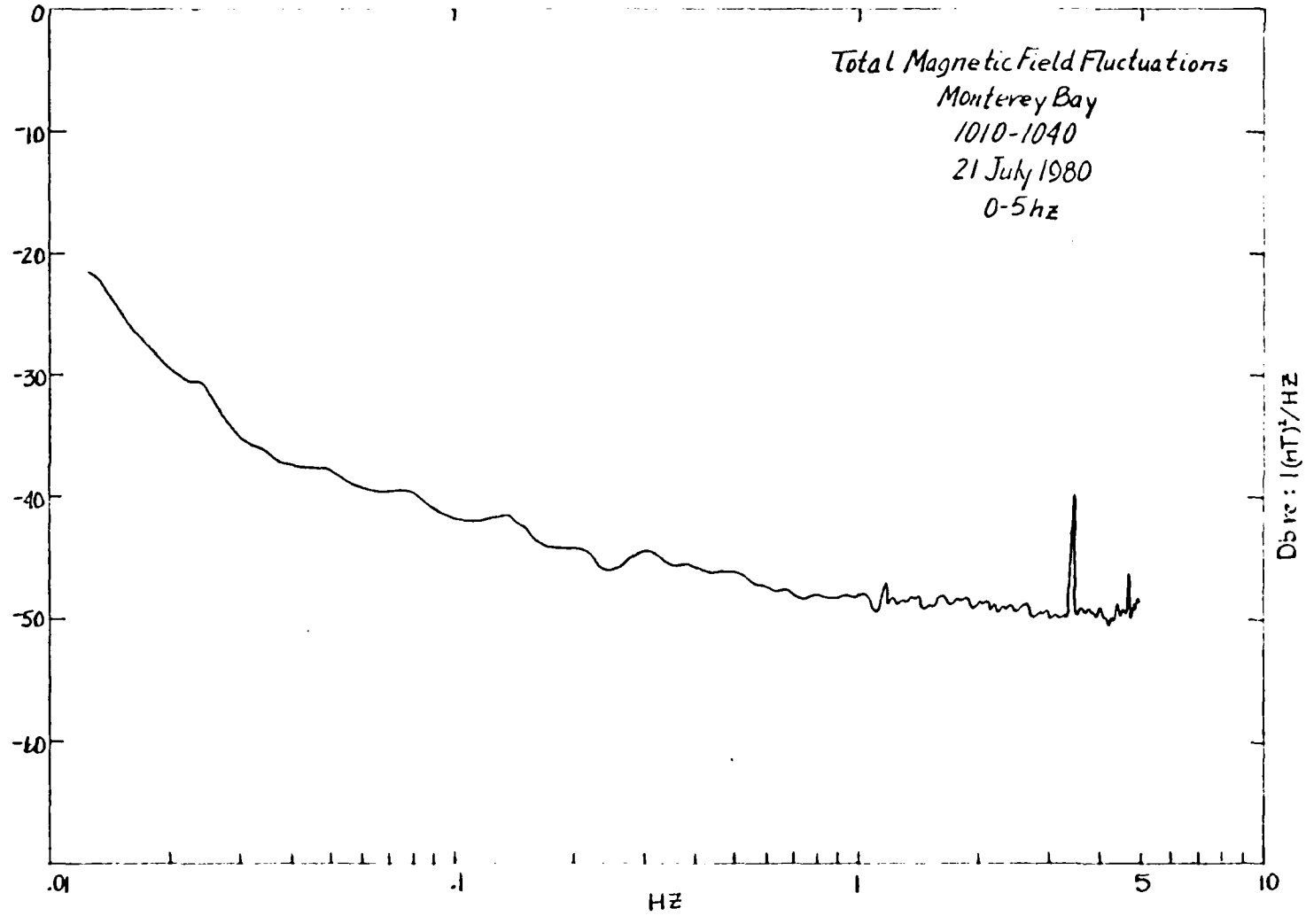
Total Magnetic Field Fluctuations
Monterey Bay
1010-1040
21 July 1980
0-5hz
0
-10
-20
-30
-40
-50
-60
.01
.1
1
5
10
Hz
Db re: 1 (nT)²/Hz

Figure 34

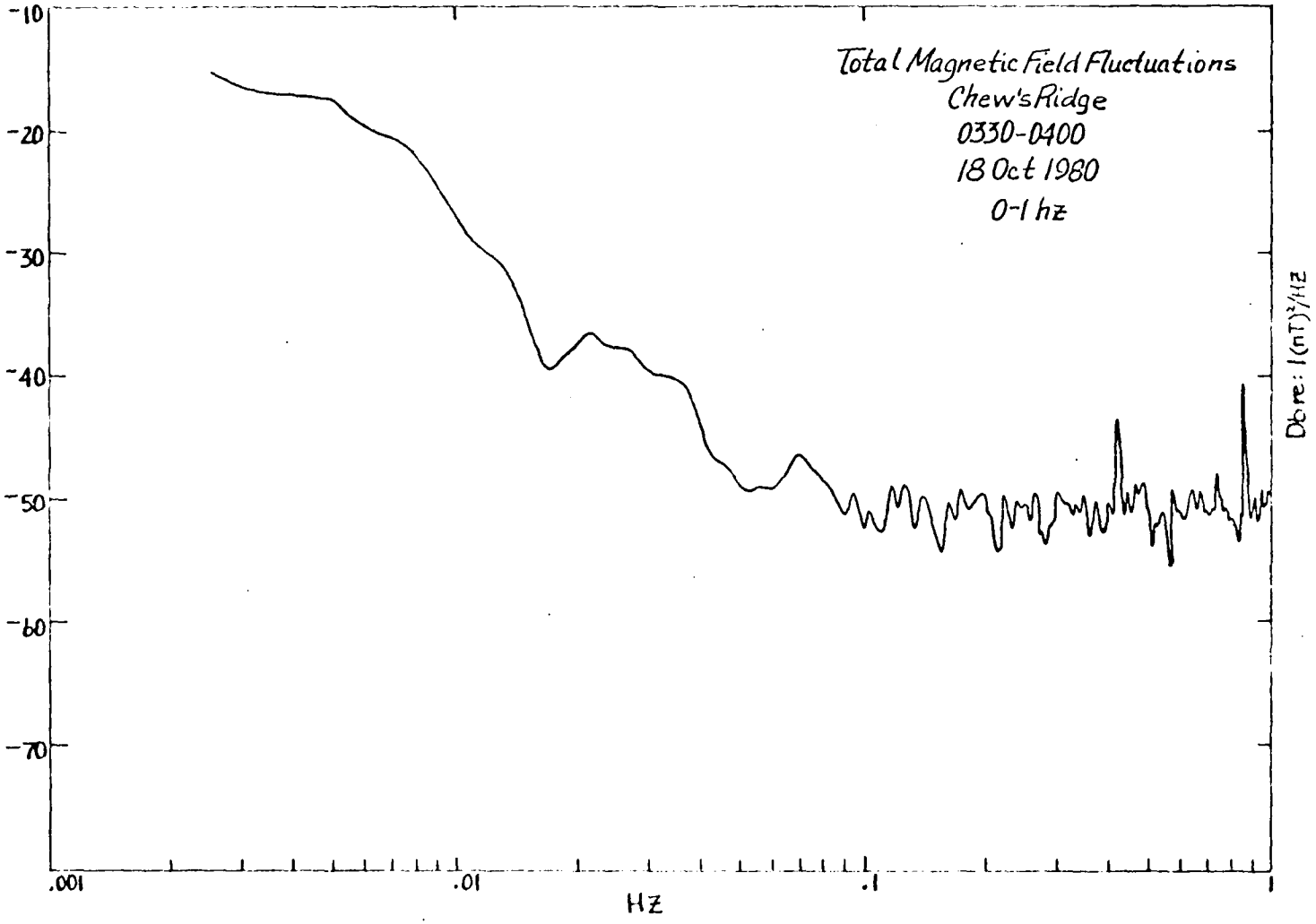
Total Magnetic Field Fluctuations
Chew's Ridge
0330-0400
18 Oct 1980
0-1 hz
-10
-20
-30
-40
-50
-60
-70
.001
.01
.1
1
Hz
Dbre: 1(nT)²/Hz

Figure 35

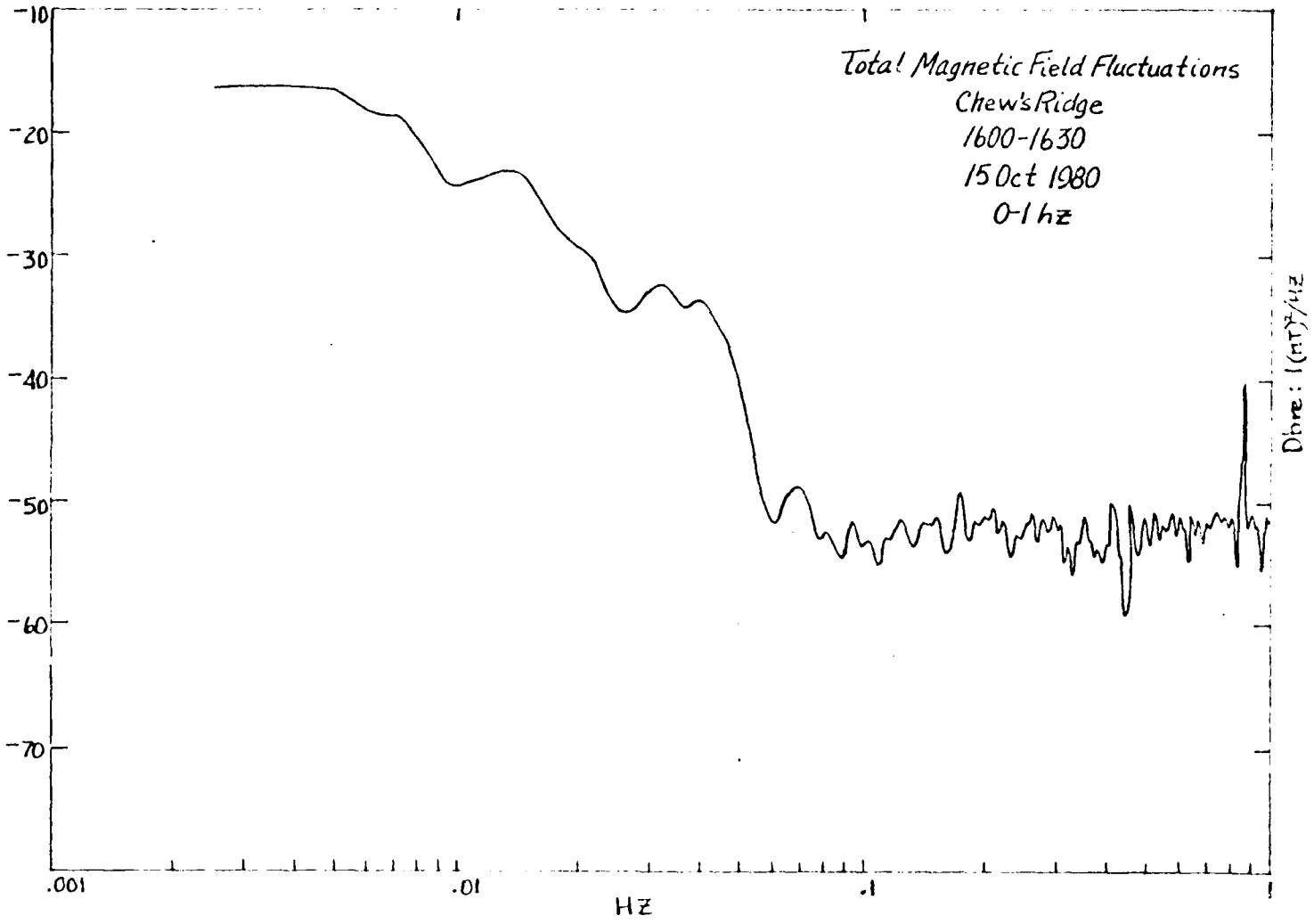
Total Magnetic Field Fluctuations
Chew's Ridge
1600-1630
15 Oct 1980
0-1 hz
-10
-20
-30
-40
-50
-60
-70
.001
.01
.1
1
HZ
Db re 1 (nT)²/Hz

Figure 36

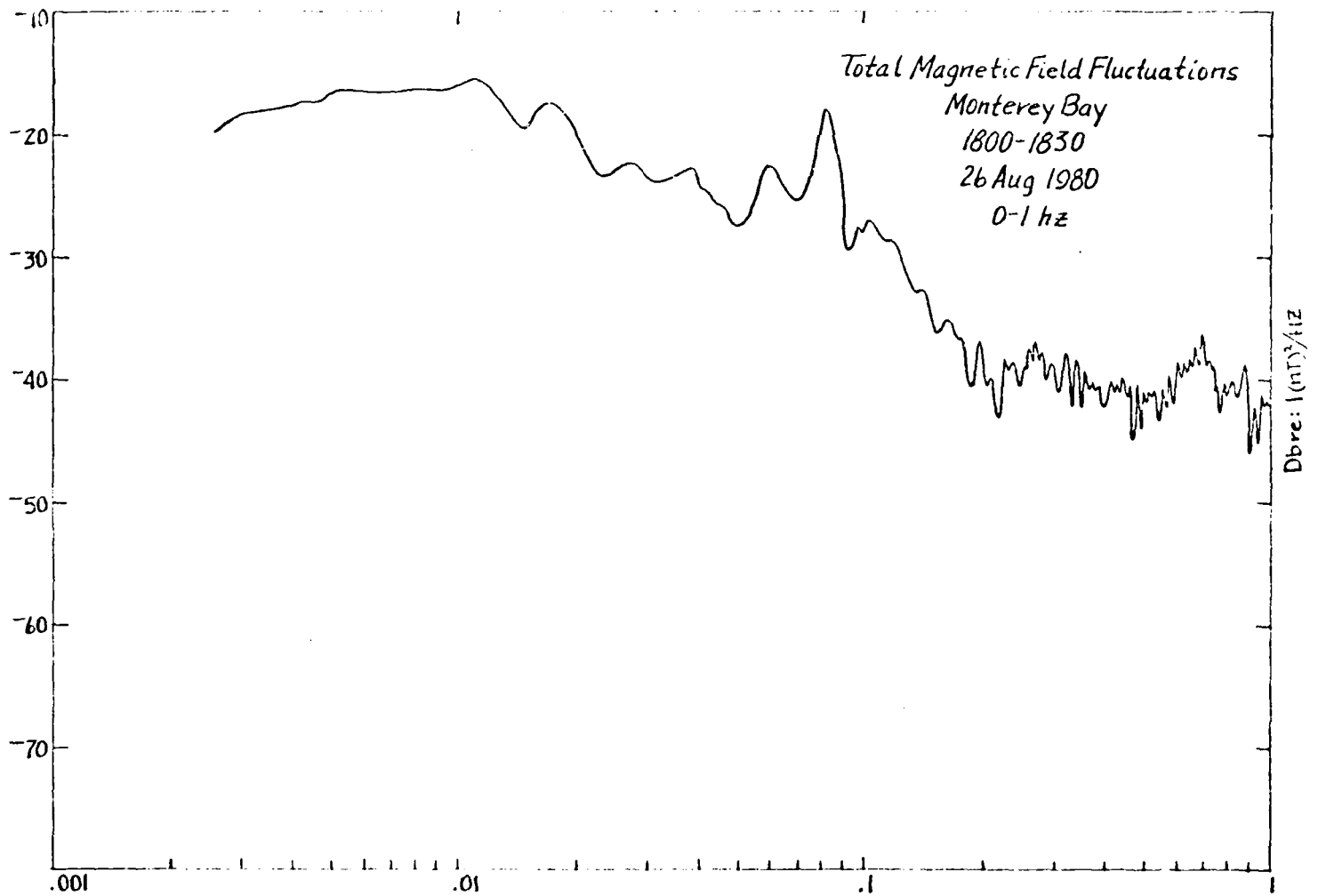
Total Magnetic Field Fluctuations
Monterey Bay
1800-1830
26 Aug 1980
0-1 hz
-10
-20
-30
-40
-50
-60
-70
.001
.01
.1
1
HZ
Dbre: 1(nT)²/Hz

Figure 37

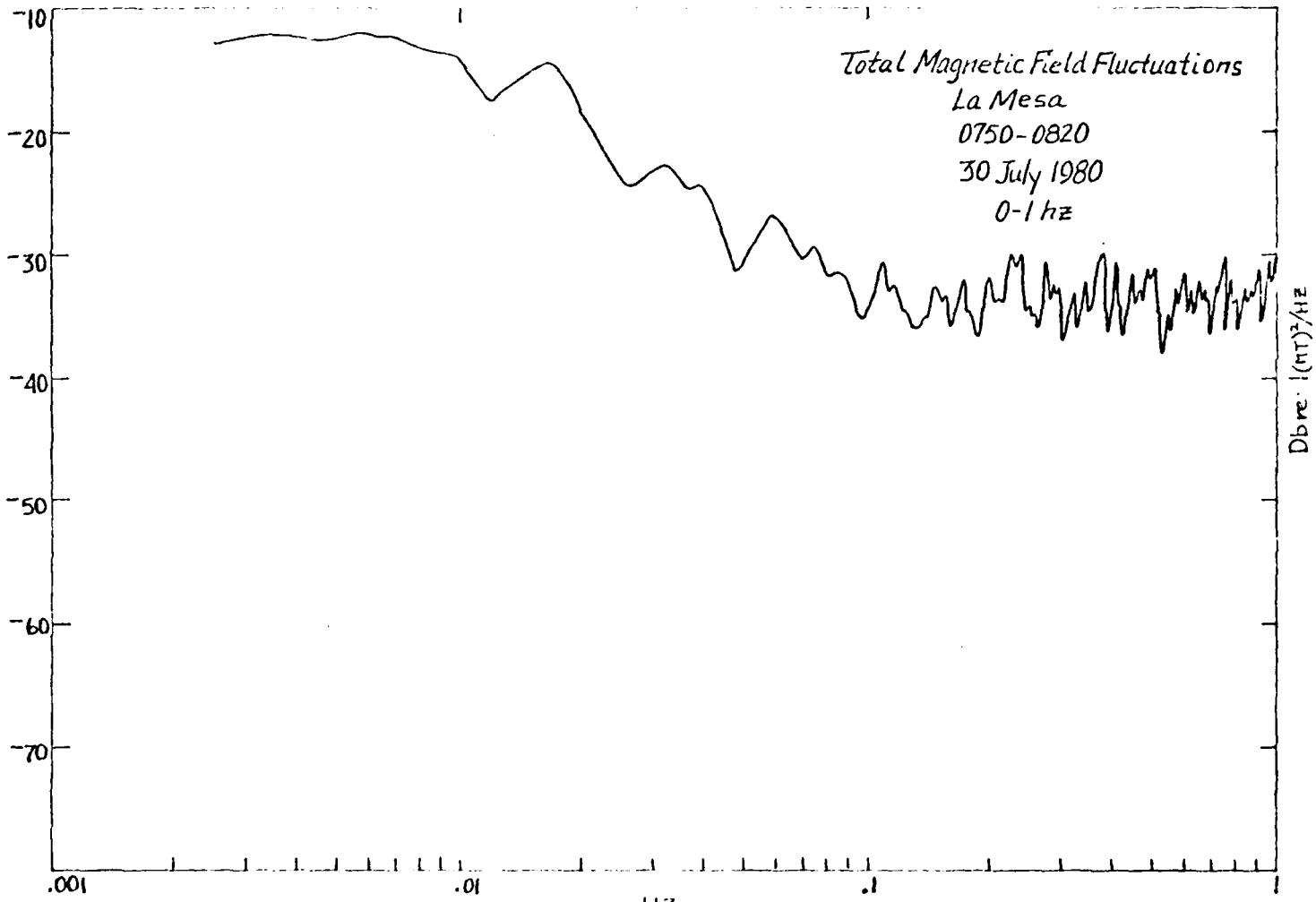
Total Magnetic Field Fluctuations
La Mesa
0750-0820
30 July 1980
0-1 hz
-10
-20
-30
-40
-50
-60
-70
.001
.01
.1
1
Hz
Dbre: 1(nT)²/Hz

Figure 38

APPENDIX C

The locations of the sea data recorded in Monterey Bay and the land data recorded at Chew's Ridge are indicated in Figures 34 to 41.

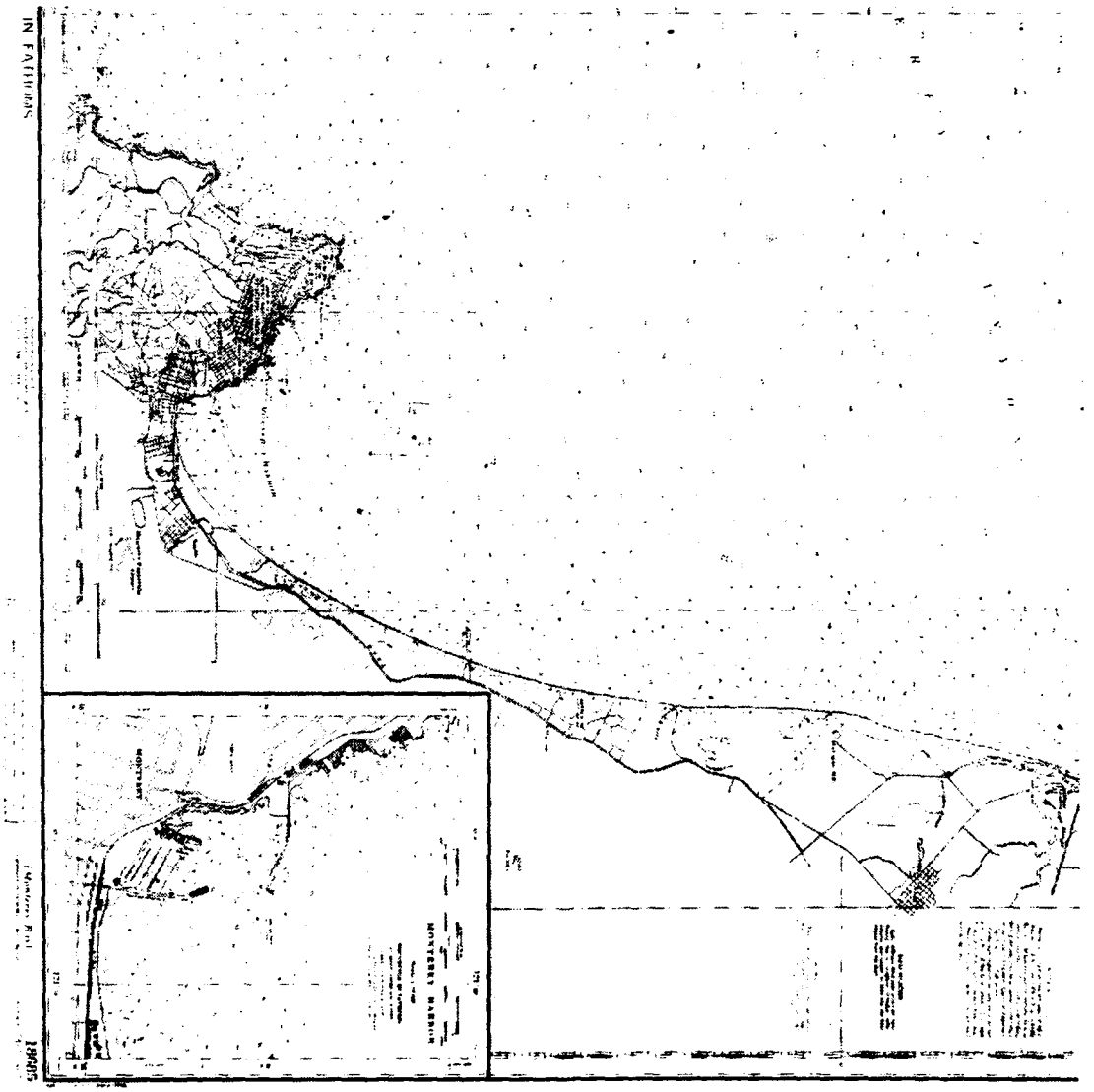

Data Collection Location, Monterey Bay

Figure 39

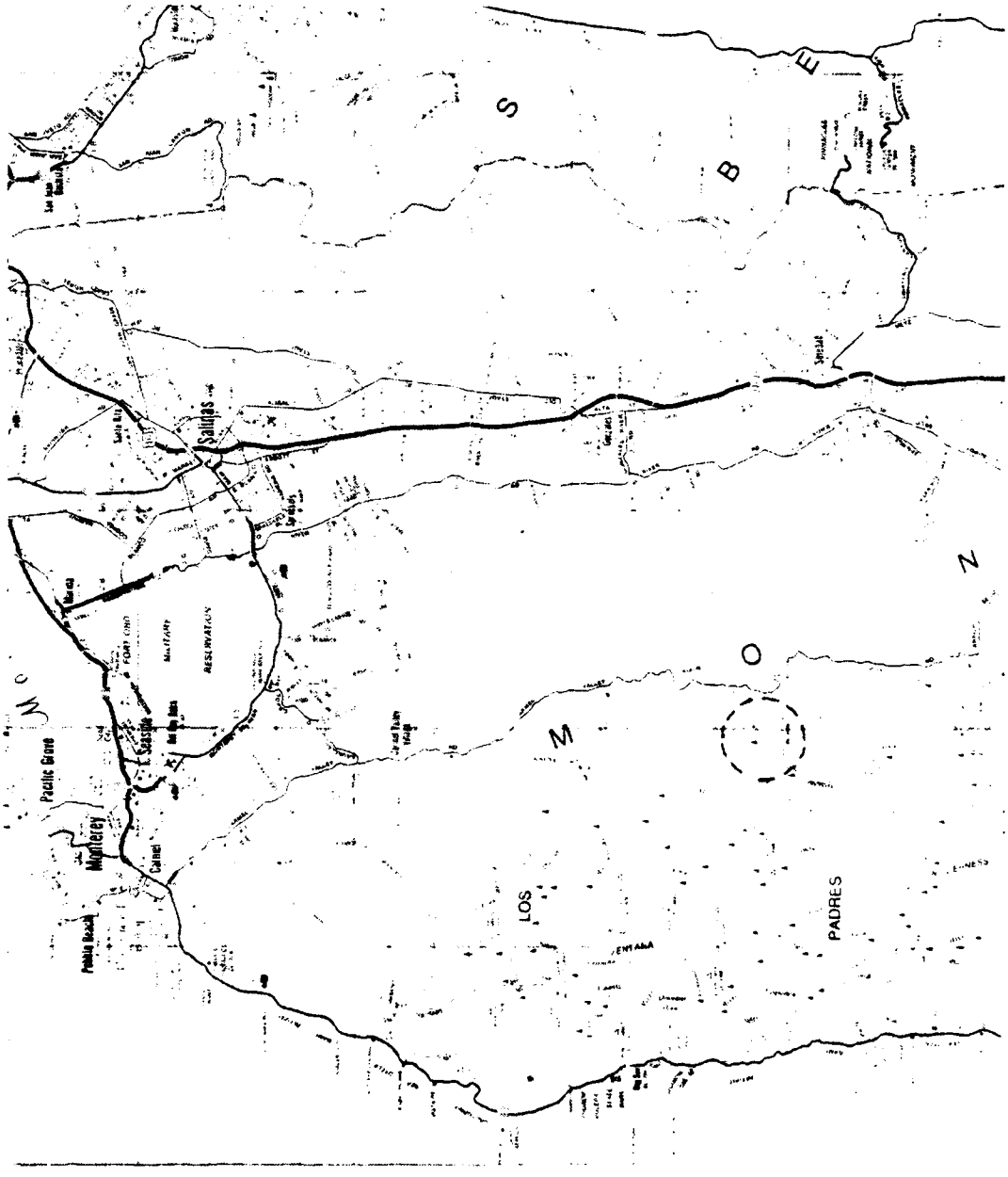

Area Map of the Land Data Collection Site

Figure 40

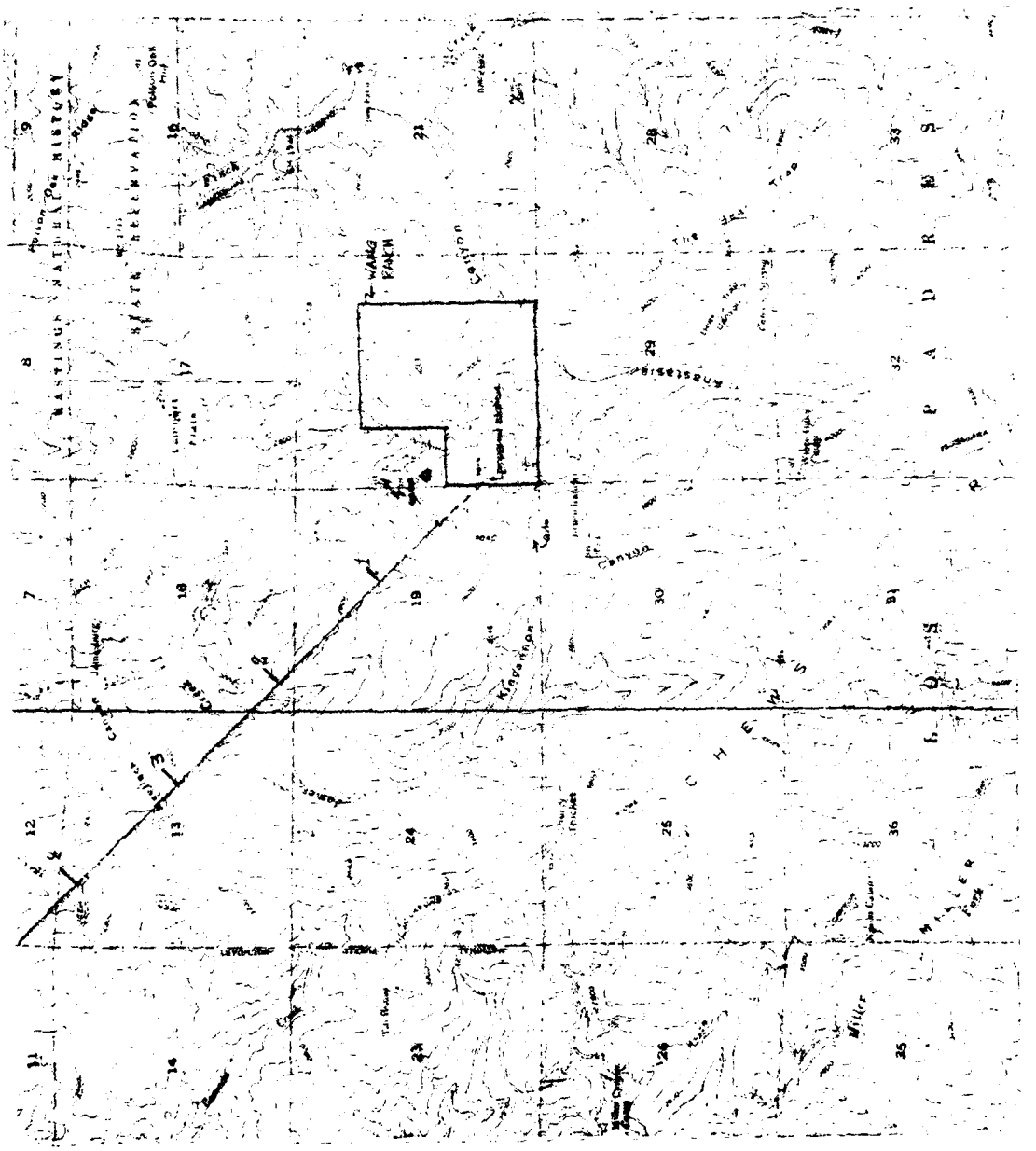

Topographic Map of the Land Data Collection Site

Figure 41

BIBLIOGRAPHY

Balser, M., Wagner, C., "Effect of a High Altitude Nuclear Detonation on the Earth-Ionosphere Cavity", Journal of Geophysical Research, V.68, No. 13, p. 4115-4118, 1963.

Barry, J.M., Power Spectra of Geomagnetic Fluctuations Between 0.1 and 10Hz, M.S. Thesis, Naval Postgraduate School, Monterey, 1978.

Campbell, W.H. and Matsushita, S., Physics of Geomagnetic Phenomena, V.1,2, Academic Press, 1967.

Chaffee, E.J., Low Frequency Geomagnetic Fluctuations (0.1 to 3Hz on the Floor of Monterey Bay, M.S. Thesis, Naval Postgraduate School, Monterey, 1979.

Clark, R.H., Allen, K.R., and Johnson, R.K., Ocean Wave Measurements with an Array of Bottom Mounted Magnetometers, Paper presented to the Geophysics Symposium in Monterey, California, 1979.

Clayton, F.W., Power Spectra of Geomagnetic Fluctuations Between 0.1 and 40Hz, M.S. Thesis, Naval Postgraduate School, Monterey, 1979.

Frasier-Smith A.C., and Buxton, J.L., "Superconducting Magnetometer Measurements of Geomagnetic Activity in the 0.1 to 14Hz Frequency Range", Journal of Geophysical Research, V.80, No. 27, p. 3141-3147, August, 1975.

Frasier-Smith, A.C., and Lee, D., "Long Term Prediction of Pc 1 Geomagnetic Pulsation Occurences", Planetary Space Science, Vo. 23, p. 431-436, 1975.

Frasier-Smith, A.C., Short Term Prediction and a New Method of Classification of Pc 1 Pulsation Occurences, Paper presented at Electromagnetic Wave Propogation in Seawater Seminar, Naval Postgraduate School, Monterey, California, 1 June, 1980.

Gordon, R.B., Physics of the Earth, Holt, Reinhart and Winston, 1972.

Herron, T.J., "An Average Geomagnetic Power Spectrum for Period Range 4.5 to 12,900 Seconds", Journal of Geophysical Research, V.72. No. 2, p. 759-761, January, 1967.

Kanamori, K., Takeuchi, H., and Uyeda, S., Debate About the Earth, Freeman Cooper and Co., 1970.

Nishida, A., Geomagnetic Diagnosis of the Magnetosphere, Springer, 1978.

Sunde, E.D., Earth Conduction Effects in Transmission, D. Van Nostrand, 1949.

Weaver, J.T., "Magnetic Variations Associated with Ocean Waves and Swell", Journal of Geophysical Research, V. 70, No. 8, p. 1921-1929, April, 1965.

Wertz, R., and Campbell, W.H., "Integrated Power Spectra of Geomagnetic Field Variations with Periods of 0.3 to 300 Seconds", Journal of Geophysical Research, V. 81, Np. 28, p. 5131-5135, 1966.

Wynn, M.J., and Trantham, H.W., A Study of the Electric and Magnetic Fields of Ocean Waves, U.S. Navy Mine Defense Laboratory Report No. 2743, 1968.

INITIAL DISTRIBUTION LIST

		No. Copies
1.	Defense Technical Information Center Cameron Station Alexandria, VA 22314	2
2.	Library, Code 0142 Naval Postgraduate School Monterey, CA 93940	2
3.	Department Chairman, Code 61 Department of Physics and Chemistry Naval Postraduate School Monterey, CA 93940	1
4.	Professor Paul H. Moose, Code 61Me Department of Physics and Chemistry Naval Postgraduate School Monterey, CA 93940	2
5.	Professor Otto Heinz, Code 61Hz Department of Physics and Chemistry Naval Postgraduate School Monterey, CA 93940	2
6.	LT G.M. McKinley 1626 Eastwood Drive Slidel, LA 70458	2
7.	LT R.M. Santos 42 Indian Run Enfield, CT 06082	2
8.	LT M. Ames SMC 1129 Naval Postgraduate School Monterey, CA 93940	1
9.	Capt. M. Beard SMC 2507 Naval Postgraduate School Monterey, CA 93940	1

10. Nick Carrera
Arms Control and Disarmament Agency 1
MA/AT
The State Department
Washington, D.C. 20451

11. Professor Ted Calhoon , Code 68
Department of Oceanography 1
Naval Postgraduate School
Monterey, CA 93940

12. Chief of Naval Research
Department of the Navy
800 North Quincy Street
Arlington, VA 22217
Code 100C1 1
Code 460 1
Code 464 1
Code 480 1

13. Commanding Officer
Office of Naval Research Branch Office 1
1010 E. Green Street
Pasadena, CA 91106

14. Director
Naval Research Laboratory 1
Code 2627
Washington, D.C. 20375

15. Office of Research, Development, Test
and Evaluation
Department of the Navy 1
Code NOP-987 J
Washington, D.C. 20350

16. Director
Defense Advanced Research Projects Agency 1
1400 Wilson Boulevard
Arlington, VA 22209

17. Air Force Office of Scientific Research
Department of the Air Force Directorate
of Physics (MPG) 1
Building 410
Bolling Air Force Base
Washington, D.C. 20332

18. Army Research Office
Department of the Army 1
Geosciences Division
Box 12211
Research Triangle Park, North Carolina 27709

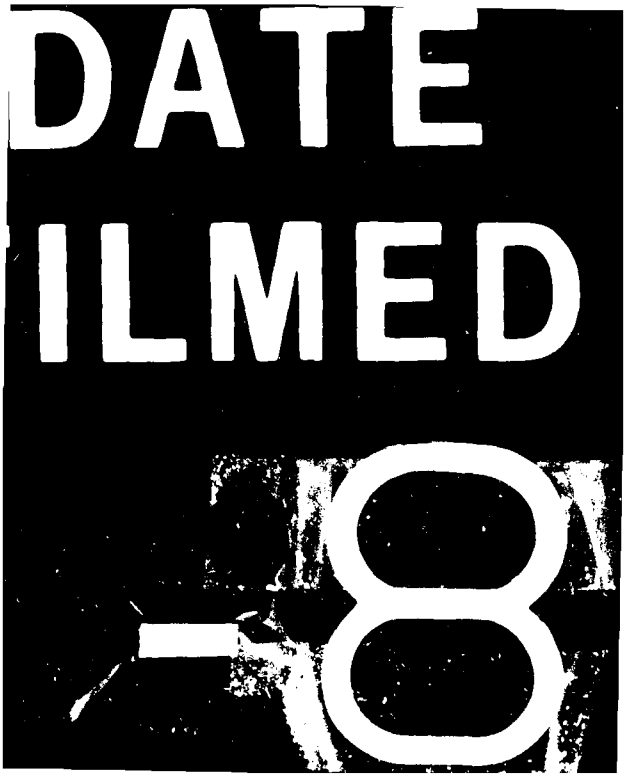
DATE
ILMED
-8